Abstract

The flexible pipelines has been widely used by the oil and gas industry the last decades and this trend is expected to continue as the operating depths are increased further. For deep water applications the radial and lateral buckling modes can be critical. Many studies has been carried out using finite element models to study these failure modes.

In this thesis a finite element model is created with the aim to recreate results obtained in a recently published article by Vaz and Rizzo. The model is built up using pipe, beam, contact and spring elements to represent the complex behaviour of the cross section. The loading is carried out by first applying the dry mass, then the external pressure and finally end compression.

When comparing buckling loads generated in this thesis by the ones in the article by Vaz and Rizzo the observation made is that the buckling loads from this thesis are significantly higher. When comparing only the inclination of the end shortening versus buckling load curves it was seen that the curves from article had a only slightly larger inclination than the results from the analyses in this thesis. This indicates that there is a small difference in the stiffness used. By modifying the stiffness it should be possible to get the same inclination of the curve.

Analyses were also carried out on how the slip distance affects the buckling loads. By increasing the slip distance by 50% and 100% it was observed that the buckling loads were reduced drastically. In the article by Vaz and Rizzo no information is given on the slip distance. By tuning the slip distance and stiffness of the springs it should therefore by possible to obtain the exact same results as in the article. This clearly illustrates the importance of stating all assumptions and input parameters when describing models used for analysis.

Scope of work

The flexible pipe represent a vital part of many oil and gas production systems. During operation of such pipes, several failure incidents may take place e.g. caused by denting and corrosion. In limit cases where inspections indicate damage, the decision making with regard to continue operations or replacing the riser may have large economic and environmental consequences. Hence, the decision must be based on accurate models to predict the residual strength of the pipe. In most applications, one or several steel layers are used to carry the hoop stress resulting from internal pressure. This is further combined with two layers of cross-wound armour tendons (typical 40-60 tendons in one layer installed with an angle of 35 ° with the pipe's length axis) acting as the steel tensile armour to resist the tension and end cap wall force resulting from pressure. For high pressure applications,local buckling of the tensile armour may occur, leading to torsion unbalance and failure of the cross-section. This thesis work is to be based on the project work performed and include the following steps.

1. Literature study, including flexible pipe technology, failure modes and design criteria, analytical methods for stress and buckling analysis of flexible pipes, non-linear finite element methods relevant for non-linear FEM codes such as MARC and the Marintek software Bflex2010.

2. Literature survey of all available literature that is relevant for the tensile armour buckling failure mode. Identify available physical/numerical test results and define associated FEM models in Bflex2010 based on the found cases.

3. Establish analytical formulas for predicting the transverse tensile armour buckling capacity considering the link between individual tensile wire failure and overall global failure in the pipe.

4. Use the FEM model to study the buckling capacity for varying curvature, external pressure and friction. Also investigate cyclic effects and result sensitivity with respect to the friction stick-slip characteristic given. Also compare with the analytical calculations.

5. Conclusions and recommendations for further work.

The work scope may prove to be larger than initially anticipated. Subject to approval from the supervisors, topics may be deleted from the list above or reduced in extent.

In the thesis the candidate shall present his personal contribution to the resolution of problems within the scope of the thesis work.

Theories and conclusions should be based on mathematical derivations and/or logic reasoning identifying the various steps in the deduction.

The candidate should utilise the existing possibilities for obtaining relevant literature.

Thesis format

The thesis should be organised in a rational manner to give a clear exposition of results, assessments, and conclusions. The text should be brief and to the point, with a clear language. Telegraphic language should be avoided.

The thesis shall contain the following elements: A text defining the scope, preface, list of contents, summary, main body of thesis, conclusions with recommendations for further work, list of symbols and acronyms, references and (optional) appendices. All figures, tables and equations shall be numerated.

The supervisors may require that the candidate, in an early stage of the work, presents a written plan for the completion of the work.

The original contribution of the candidate and material taken from other sources shall be clearly defined. Work from other sources shall be properly referenced using an acknowledged referencing system.

The report shall be submitted in two copies:

- Signed by the candidate
- The text defining the scope included
- In bound volume(s)
- Drawings and/or computer prints which cannot be bound should be organised in a separate folder.

Ownership

NTNU has according to the present rules the ownership of the thesis. Any use of the thesis has to be approved by NTNU (or external partner when this applies). The department has the right to use the thesis as if the work was carried out by a NTNU employee, if nothing else has been agreed in advance.

Thesis supervisors

Prof. Svein Sævik, NTNU.

Preface

This report is the result the Master's thesis work for stud.techn. David Nygård during the spring semester 2012 at the Department of Marine Technology, Norwegian University of Science and Technology. The work has been based on the project work performed in the fall of 2011.

During the early stages of the thesis work a lot of time were spent trying reading available literature in the field of flexible pipes and to learn the BFLEX2010 software and how it is used to generate the flexible pipe models. In addition a lot of time was spent generating Matlab-scripts to run multiple analysis and generating multiple plots automatically. As a result of this the analysing of the created models were started a bit late.

When starting to interpret the results of the analyses it was discovered that the results did not follow what would be expected. It was assumed that this was a result of how the external pressure was applied. This lead to a lot of time being spent trying different ways of applying the external pressure in order to get results that seemed reasonable.

Later it was discovered that the number of elements had a large influence on the results. Even though the element lengths originally were chosen below the critical length for Euler buckling it was discovered that when doubling the number of elements from 100 to 200 the results seemed to be more reasonable. Had this been discovered at an earlier stage a lot of the time spent modelling the external pressure could have been used investigating other interesting effects.

Generating the models, understanding the theory behind the models and interpreting the results from the analyses has been both challenging and time consuming. Frustration has been experienced when the results were not as expected, but all in all the thesis work has been both interesting and informative.

I would really like to thank my professor and supervisor Svein Sævik for the help he has offered me when working with this thesis. His knowledge and insight into the field of flexible pipes and modelling of flexible pipes has been invaluable for the completion of this thesis. I would also like to thank my co-students for sharing their experiences from working with similar problems.

Trondheim, June 10th, 2012

David Nygård

Summary

The flexible pipelines has been widely used by the oil and gas industry the last decades and this trend is expected to continue as the operating depths are increased further. The flexible pipe is built with a composite wall structure where helical armouring layers and polymer sealing layers are the main components. This leads to the pipe having both a low bending stiffness and high axial stiffness.

A possible failure mode for the tensile armour wires in deep water applications is radial buckling which may result from high axial compression or torsional failure. One solution to prevent this is to use a high strength tape around the tensile armour wires. If the radial movement is sufficiently restrained the wires are forced to move laterally and lateral buckling may occur. Mechanisms triggering lateral buckling have been found to be the reverse end cap effect, damaged outer sheath and repeated bending cycles.

Many studies have been carried by using finite element models trying to capture the effects leading to buckling in the flexible pipe armour wires. In a recently published article by Vaz and Rizzo the instability of the flexible pipe armour wires were investigated by varying the external pressure and friction factors using a finite element model. Both the radial and lateral buckling modes were detected. In another recently published study the radius of curvature were varied in addition to exposing the wires to cyclic bending. Two different forms of lateral buckling were detected in the pipes using both a finite element model and experimental studies.

A finite element model was created based on the information given in the article by Vaz and Rizzo. The goal was to recreate the results by running the same analyses using the BFLEX2010 software. As not all information on the model used in the article was given some key parameters and details of the model had to be assumed in order to create the new model.

The model created was e flexible pipe with length of 4.98 meters and three pitches of tensile armour wires with a lay angle of 30°. The cross section of the armour wires were 3 x 10 mm. The model was built up using different pipe, beam, contact and spring elements in order to recreate the complex behaviour of the flexible pipe cross section. The model was exposed to loading in three steps. First the dry mass were added, then the external pressure and finally end compression.

For applying the external pressure three different approaches were used. The pressure was applied as nodal point loads on springs connected to the outer wire, nodal point loads on springs connected to the inner wire and as pre described displacements on the outer wire.

Sensitivity studies were also carried out concerning the length of the time interval for applying the external pressure, how many elements to be applied and if the magnitude of the pre described displacements on the end affected the results. From these studies it was decided that a time interval of 10 seconds for applying the external pressure was sufficient. It was also assumed that using 200 elements was sufficient and that applying a pre described displacement of 12.5 mm did not affect the results compared to using 2.5 mm.

By varying how the external pressure was applied three different models were used for the analysis. In addition analyses were carried out on the same models

when they were restrained from torsion resulting in a total of 6 different cases. For each case the analyses were carried out varying the external pressures and friction factors in the same way as in the article by Vaz and Rizzo.

When comparing the three first cases were torsion of the pipe was allowed it was observed that the buckling loads were quite similar. The buckling of the wires seemed to be initiated at the end of the pipe. When comparing the three first cases allowing for torsion with the three next cases restrained from torsion the results were quite similar for the lowest friction factors. For the higher friction factors the maximum buckling loads were increased indicating that buckling may not be as a result from torsion for these cases. Again it was observed that the wire buckling seemed to be initiated at the end of the pipe.

Compared to the buckling loads in the article by Vaz and Rizzo the buckling loads obtained by the new analyses were significantly higher. In order to compare the results more accurately the inclination of the end shortening versus buckling load curves were compared. The curves from the article had an inclination of 5.3 and the curves obtained from the BFLEX2010 analyses were slightly lower. This indicates that a different stiffness has been used for the respective models.

Some analyses were also carried out on how the slip distance affects the buckling loads. By increasing the slip distance by 50% and 100% it was observed that the buckling loads were reduced drastically. In the article by Vaz and Rizzo no information is given on the slip distance. By tuning the slip distance and stiffness of the springs it should therefore by possible to obtain the exact same results as in the article. This clearly illustrates the importance of stating all assumptions and input parameters when describing models used for analysis.

Sammendrag

Fleksible stigerør har vært veldig mye brukt innen olje og gass industrien de siste tiårene og denne trenden forventes å fortsette fremover. Tverrsnittet til det fleksible stigerøret er bygd opp av forskjellige lag med ulike egenskaper. Strekkarmeringen er en viktig komponent i denne sammenhengen. På grunn av det komplekse tverrsnittet til det fleksible stigerøret har det både lav bøyestivhet og høy aksialstivhet.

Når det fleksible stigerøret blir brukt på store havdyp kan det oppleve knekning i radiell retning når det blir utsatt for høy aksialkompresjon eller torsjon. En løsning for å unngå dette er å bruke en kraftig tape rundt strekkarmeringen. Dersom den radiale knekkformen blir forhindret blir strekkarmeringen tvunget til å bevege seg lateralt og en lateral knekningsform kan oppstå. Mekanismene som utløser lateral knekning er den motsatte "end-cap" effekten, skadet ytre lag eller gjentatte bøyesykluser.

Mange studier har blitt utført ved hjelp av FEM-modeller for å utforske effektene som fører til knekning i strekkarmeringen til det fleksible stigerøret. I en nylig utgitt artikkel av Vaz og Rizzo ble knekning av strekkarmering undersøkt med å variere ytre trykk og friksjonsfaktoren på en FEM-modell. Både lateral og radial knekning ble oppdaget. I en annen nylig studie ble en effektene av forskjellig kurvaturradius og syklisk bøyning undersøkt. To ulike former av lateral knekning ble oppdaget i strekkarmeringen både for FEM-modellen som ble undersøkt og for eksperimenter på et tilsvarende rørtverrsnitt.

Basert på informasjonen gitt i artikkelen av Vaz og Rizzo ble en tilsvarende FEM-modell laget. Målet var å gjenskape resultatene med å utføre de samme analysene i BFLEX2010. Siden ikke all nødvendig informasjon for modellen var gitt måtte en del verdier og detaljer for modellen antas.

Modellen som ble laget var et fleksibelt stigerør med lengde 4.98 meter og tre pitcher med knekkarmering med en leggevinkel på 30°. Tverrsnittet til strekkarmeringen var 3 x 10 mm. Modellen ble bygget opp av forskjellige rør, bjelke, kontakt og fjær elementer for å gjenskape den komplekse oppførselen til tverrsnittet i det fleksible stigerøret. Modellen ble utsatt for last i tre steg. Først ble den tørre massen påsatt, deretter ble røret utsatt for ytre trykk og til slutt ble enden av røret påført kompresjon.

For å sette på det ytre trykket ble tre tilnærminger brukt. I det ene tilfellet ble trykket påsatt som en punktlast på fjærene koblet til den ytre strekkarmeringen. I det andre tilfellet ble trykket påsatt som en punklast på fjærer tilkoblet den indre strekkarmeringen. I det siste tilfellet ble den ytre strekkarmeringen påsatt en foreskrevet forskyvning tilsvarende kraften på til det ytre trykket.

Sensitivitetsstudier ble også utført med tanke på lengden av tidsintervallet som brukes for å sette på det ytre trykket. I tillegg ble det undersøkt hvor mange elementer som burde brukes og hvor stor den foreskrevne forskyvningen som påføres enden av røret bør være. Ut fra dette ble det konkludert med at tidsintervallet som brukes for å sette på det ytre trykket var tilstrekkelig. I tillegg ble det antatt at bruk av 200 elementer ville gi akseptable resultater og at påsetning av en endeforskyvning på 12.5 mm ikke påvirket resultatene sammenlignet med å sette på en endeforskyvning på 2.5 mm.

Ved å variere hvordan det ytre trykket ble påsatt modellen måtte vi analysere tre ulike tilfeller. I tillegg ble det utført analyser på den samme modellen både med og uten å tillate torsjon på røret. Totalt ble derfor seks ulike tilfeller undersøkt. For hvert tilfelle ble analysene utført på samme måte som i artikkelen til Vaz og Rizzo med tanke på hvordan ytre trykk og friksjonsfaktor ble variert.

Ved å sammenligne de tre første tilfellene der torsjon av røret var tillatt ble det observert at knekklastene var ganske like. Det ble også observert at knekningen så ut til å begynne på enden av røret. Når tilfellene med og uten torsjon ble sammenlignet viste det seg at resultatene var bortimot identiske for de laveste friksjonsfaktorene. For de høyere friksjonsfaktorene var knekklastene noe høyere, noe som indikerer at de knakk på grunn av torsjon for de tre første tilfellene der dette var tillatt. Igjen ble det oppdaget at knekningen så ut til å begynne på enden av røret.

Sammenlignet med knekklastene i artikkelen av Vaz og Rizzo var knekklastene i de utførste analysene mye høyere. For å sammenligne resultatene mer presist ble stigningen på endeforkortelse versus knekklastene sammenlignet. Det viste seg at kurvene fra artikkelen hadde et stigningstall på 5.3 mens stigningstallet til de utførte analysene var litt lavere. Dette indikerer at forskjellig stivhet har blitt brukt i modellen som ble laget sammenlignet med den som ble brukt i artikkelen.

Analyser ble også utført for å undersøke effekten på knekklastene ved å øke lengden strekkarmeringen har lov å gli før friksjon blir aktivert. Ved å øke denne med 50% og 100% ble knekklastene redusert kraftig. I artikkelen til Vaz og Rizzo står det ingen informasjon om hvor langt strekkarmeringen har lov til å gli før friksjonen spiller inn. Ved å kalibrere denne lengden og stivheten som ble brukt bør det være mulig å gjenskape kurver med nøyaktig samme stigningstall og knekklaster som i artikkelen til Vaz og Rizzo. Dette understreker viktigheten av å oppgi alle antagelse og parametere for modellen som blir brukt når analyser blir utført.

Contents

List of Figures

List of Tables

Nomenclature

Abbreviations

DOF	Degree of freedom
FE	Finite element
FEM	Finite element method
SBM	Sandwich Beam Theory

Greek letters

α	Lay angle of the armour wires
α_e	Lay angle of the inner armour wires
α_i	Lay angle of the outer armour wires
β_b	Parameter governing the first buckling mode
γ	Shear deformation parameter
β ,β_i	Relative displacement vector and its component in direction i
Δ	Important parameter governing ku
ϵ_1	Axial strain of a wire
ϵ_p	Axial strain of the pipe
$\epsilon(\mathrm{t})$	Axial strain of a wire as a function of time
$\epsilon_{10-19}(\mathrm{t})$	Axial strain of a wire between 10 and 19 seconds
$\epsilon_{20-101}(\mathrm{t})$	Axial strain of a wire between 20 and 101 seconds
$\Delta\epsilon$	Change in axial strain for time period of 10 seconds
$\Delta\epsilon_{20}$	Modified strain after 20 seconds
μ	Friction factor
σ_E	Euler buckling stress
τ_f	Available friction force between the wires
τ_p	Shear force in the pipe
ω_i	Torsion and curvature deformation components

Roman letters

A_{pipe}	Total area of the flexible pipe model
b , h	Width / height of single armour wire element
c , $\mathbf{c}$	Shear interaction parameter/tensor
E	Elastic modulus of material
EA	Axial stiffness of the wire
F_j	Fill factor determining the gaps between armouring wires
$F_{x,compared}$	Force recorded in model after modification
$F_{x,original}$	Force recorded in model
F_{pipe}	Force applied to flexible pipe model in order to simulate external pressure
F_{spring}	Force in spring
$F_{z,e}$, $F_{z,i}$	Force recorded in external and internal wires in article by Vaz and Rizzo
F_z	Force recorded by model used in article by Vaz and Rizzo
ΔF_{10-20}	Change in force between 10 and 20 seconds
ΔF_{20-30}	Change in force between 20 and 30 seconds
G	Shear modulus
I_i	Cross section constants
k	Shear stiffness parameter
K	Buckling factor dependant upon boundary conditions
k_u	Pre slip stiffness governing the buckling parameter β
k_{spring}	Stiffness of spring
L	Total length of pipe
L_e	Length of single armour wire element
L_{pipe}	Length of the flexible pipe model
n_i	Total number of wires in each layer
P	External loading
P_E	Euler buckling load
P_{ext} , P_{int}	External / internal reaction force
P_{m1}	Buckling load corresponding to the first buckling mode
R	The radius of the pipe
t	Thickness over which the deformation of the wire occur
$\mathbf{u}$,u_i	Displacement vector and its component in direction i
u_{1p}	Wire displacement what would occur if plane surfaces remain plane after bending deformation
u_3	Displacement in the local z-direction of the wire
u_s	Actual longitudinal displacement along the wire
u_{spring}	Displacement of spring
W_i	Internal work

1 Introduction

Flexible pipelines can be used for operation from both fixed and floating structures, whereas the rigid pipelines may only be used for fixed structures. This is one of the reasons why the flexible pipelines has been widely used by the oil and gas industry in the last decades. Another reason is that the water depth for operation has been increasing making the use of floating productions units necessary. As new fields in Brazil and Gulf of Mexico are reaching depths of 2500 to 3000 meters the flexible pipe are expected to be even more important in the future.

For deep water applications the flexible pipeline may experience large external pressures and sometimes also bending. If the flexible pipe is not designed properly it may not be able to withstand the loading and failure may occur. Failure of the flexible pipe can be critical since it may result in large spills before the failure is discovered. This illustrates the importance of designing the flexible pipe in a way making it able to withstand all loading it is exposed to without failing.

Accurate models of local buckling are very important in order design the flexible pipe in a correct manner. As the water depths are increasing the costs of full scale experiments to investigate buckling would be very high. This makes the use of finite element models able to predict the different buckling more and more important.

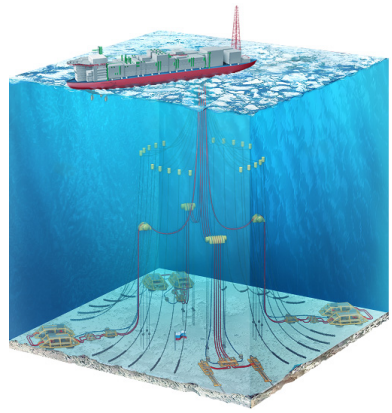

Figure 1.1: System of flexible pipelines

In agreement with the supervisors the focus of this thesis has been to investigate the buckling capacity for varying external pressures and friction factors by creating a finite element model. The goal for the model was to be able to recreate the results in a recently published article.

1.1 Build up of thesis

In **Chapter 2** the flexible pipe is briefly introduced by presenting its main applications and configurations. The cross section of the flexible pipe is described in detail and the most important design criteria are presented along with the most important failure modes.

Chapter 3 is a short literature survey of available literature where physical or numerical test results and associated FEM-models have been presented. The chapter gives a short summary of two recently published articles focusing how the FEM-models are created and the results obtained.

The theory behind the FEM software used for the analyses in this thesis are presented in **Chapter 4**. The software and its theoretical foundations are described briefly before some element types are presented in more detail. The chapter also contains analytical formulas for buckling focusing on how the slip distance affects the buckling loads.

Chapter 5 contains the most important assumptions and details of the FEM-model created. The build up of the model is described with regard to tensile armour wires, element length, nodal points, element properties, boundary conditions, loading and the friction model.

The details of how the analyses are carried out and presented are found in **Chapter 6**. The chapter contains information on the programs used, how input parameters are varied and implemented into input files and how the analyses are executed. Some descriptions are also given on how the results from the analyses are processed and presented.

In **Chapter 7** some modelling sensitivity analyses are carried out to investigate how certain parameters affect the results. Based on the results some assumptions are made and implemented into the model created in chapter 5.

The results of the analyses carried out are presented in **Chapter 8**. The results are split into different cases depending on how the external pressure is applied and if torsion is allowed or not. The results are also compared to the results in the article by Vaz and Rizzo.

Conclusions from the work carried out in this thesis and recommendations for further work can be found in **Chapter 9** .

2 The flexible pipe

2.1 Applications and configurations

The flexible pipes are widely used by the oil and gas industry in different applications such as flowlines, fixed jacket risers or risers connected to floating production units. The basic requirements for the flexible pipe is long lifetime, mechanical strength, internal and external damage resistance and minimal maintenance. If the application involves dynamic behaviour it is also important that the pipes have high pliancy and high fatigue resistance [4].

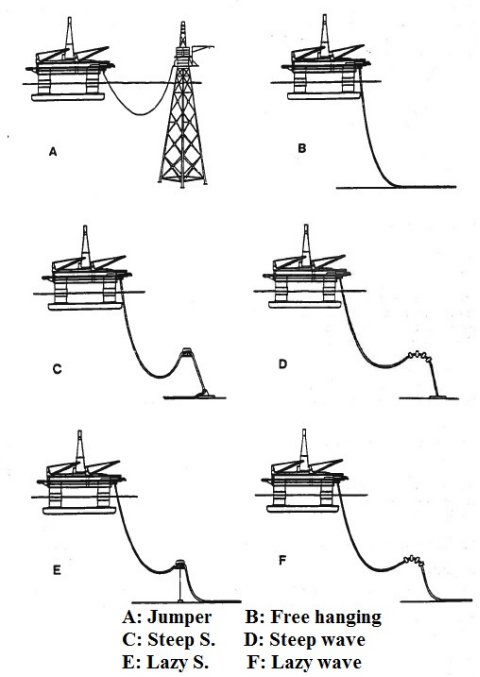

Figure 2.1: Commonly used flexible riser configurations [10]

For flexible pipes used as fully dynamic risers in fixed and floating offshore production systems there are some commonly used standard configurations as seen in figure 2.1. Which configuration to use depends on the local environmental conditions, floater motions, water depth, number of risers, bottom arrangement of risers and the cost of the solution. There is no objective procedure on how to select the configuration, so often experience and engineering judgements are important in this process.

2.2 Cross section

The flexible pipe is built up with a composite wall structure where helical armouring layers and polymer sealing layers are the main components. This leads to the pipe having both a low bending stiffness and high axial tensile stiffness, allowing for a much smaller radius of curvature compared to classical steel pipes [4].

Flexible pipe cross sections can be termed as either bondened or unbondened. The bondened cross section is characterized by the layers beeing bonded together by a vulcanized layer. As a consequence of this the layers are not able to move relative to each other. For the unbondened cross section the vulcanized layer is skipped, and the layers are able to move relative to each other.

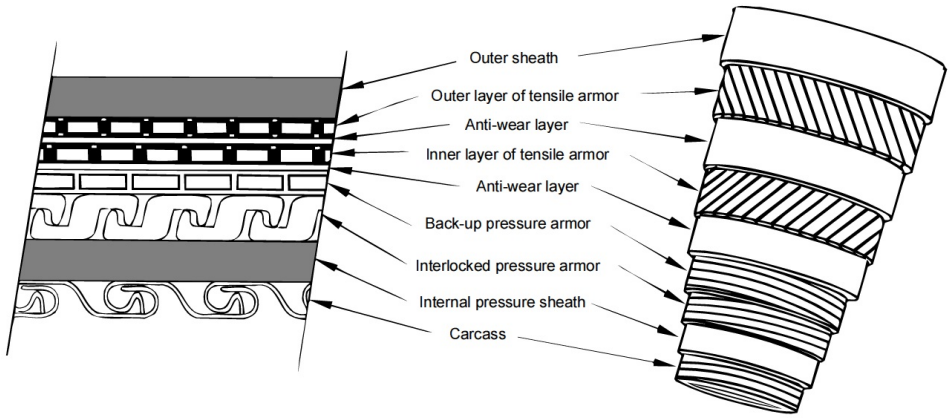

Figure 2.2: Description of the unbondened cross section [4],

2.2.1 Unbondened flexible pipe wall structure

The unbondened flexible pipe is built up from several structural layers each with different functions as seen in figure 2.2. The two innermost layers are the plastic sheath and the carcass. The plastic sheath is needed to safely transfer the internal fluid without loss. Since the plastic sheath has a very limited ability to withstand the external pressure a carcass is needed to prevent collapse.

Outside the plastic sheath there is one or two layers of pressure armour. The purpose of these layers is to withstand the radial forces caused by internal and external pressure. The interlocked pressure armour is a wound steel spiral used for both high and low pressure applications. The second pressure armour layer is a flat steel carcass used for very high pressure applications [12].

Outside the pressure armour the inner tensile armour wires are resting on an anti wear layer providing friction for the tensile wires. An anti-wear layer is also situated between the wire layers providing friction for the outer armour wire layer. The purpose of the tensile armour wires is to provide axial and torsional capacity of the pipe. Usually the tensile armour consists of 40-60 steel wires in each layer.

The wires are cross-wound an angle between 20 ° to 60 °. The angle depends on the required strength characteristics of the pipe, but typically a 35 ° angle is used to get an torsionally balanced pipe.

Outside the tensile armour wires a plastic sheath is located to protect the pipe from corrosion and to bind the underlying layers. Depending on which of the layers in figure 2.2 are being used the unbondened flexible pipe can be divided into different categories. To get a smooth-bore pipe the inner steel carcass is neglected, while for a rough-bore pipe the pressure armour layer and intermediate sheath is removed.

For higher pressure applications the rough-bore reinforced pipe is used. This has a cross section consisting of all the layers in figure 2.2 and in addition a high strength tape is applied between the outer tensile armour wire and the outer plastic sheath. The purpose of the high strength tape is to avoid the wires from moving radially outwards.

Figure 2.3: Unbondened cross section with four tensile armour wires [3].

Another variation of the cross section being used for very high pressure applications is to add two extra layers of cross wound tensile armour wires in addition to the high strength tape as seen in figure 2.3.

2.3 Design criteria

For a successful design of flexible pipes several criteria must be fulfilled. The unbondened flexible pipe design criteria are strain, creep, stress, hydrostatic collapse, mechanical collapse, torsion, crushing collapse, compression and service life factors [4].

Many of the design criteria include a utilization factor representing the ratio between the structural capacity and the applied load. The utilization factor is used to include the effects the uncertainties involved in the design process and is therefore often given with a value well below 1.

Creep is an issue for the internal pressure sheath as this can creep into the pressure layer or the tensile armour layer under normal service conditions resulting in leakage. This can be avoided by designing the wall thickness to account for creep.

The design stress should be defined using an utilization factor based on the material capacity in order to have acceptable safety against failure. It should also account for residual wire stress.

The flexible pipe will experience torsional loads both under installation and under service and should have enough torsional strength to withstand this without any structural damage. Maximum allowable torsion is derived from two scenarios. For the first scenario torsion is applied resulting in the outer tensile armour wire turning inwards. The tensile forces resulting from this should not exceed the allowable stress. For the other scenario the torsion is applied in the other direction resulting in a gap between the tensile armour wires. The damaging torsion is now set to the force needed to make a gap equal to half the thickness of the tensile armour wire [4].

Under installation the flexible pipe may experience large tension loads and chrushing effects both when reeling or unreeling and from the controlling tensioner. The collapse load should be calculated based on the resistance of the internal carcass and supporting layers.

Compression of the flexible pipe can be divided in two categories. In the first category effective compression can lead to increased deformation in the pipe. The effective compression is not to cause bar buckling of the pipe or violation of the MBR criteria stated in ISO 13628-2 [5].

The other compression category is axial compression. This causes a gap between the tensile armour wires. The maximum axial compression allowed will be the value leading to a gap equal to half the thickness of the tensile armour wires. In addition an analysis on tensile wire buckling should be performed.

Detailed information on the design criteria for flexible pipes can be found in ISO 13628-2 [5] and API RP 17B [4].

2.4 Failure modes

For the flexible pipe failure means that the pipe is no longer capable of transferring the internal fluid in a correct manner. The flexible pipe must be designed to be able to satisfy the functional requirements when exposed to both functional loads, environmental loads and accidental loads. Different parts of the flexible pipe cross section may experience different failure modes [4].

If the internal pressure is large enough the tendons in the tensile armour wires may experience a rupture. This is termed burst. Possible design solutions for the wires against burst is to change the shape, increase the thickness, change the material or to add additional layers of tensile armour wires.

Figure 2.4: Rupture of the tensile armour wires of a flexible pipe [6].

The wires may also experience tensile failure if the tension is large enough. Solutions for this is either to increase the tendon thickness or to change the material. The same tensile failure may be the result is the torsional forces are large enough. If this is the case the solution is to modify the system to reduce the torsional loads.

Fatigue may also be a problem for the wires. If the fatigue loads can not be reduced the alternatives are to increase wire thickness or change the material. Corrosion will occur in the wires if exposed to seawater. This can be prevented by cathodic protection, modified material, increased layer thickness or extra coating.

Two of the failure modes currently subject to a number of both academic and industrial investigations are the radial and lateral buckling of the tensile armour wires.

2.4.1 Radial buckling of tensile armour wires

Radial buckling of the tensile armour wires is a well known failure mode for the flexible pipe and it is often referred to as "bird caging". This may be a problem for deep water applications due to the resulting high axial compression on the flexible pipe. The compression may lead to instability in the tensile armour wires and they may deflect in the radial direction creating the classical "bird-cage" as can bee seen in figure 2.5.

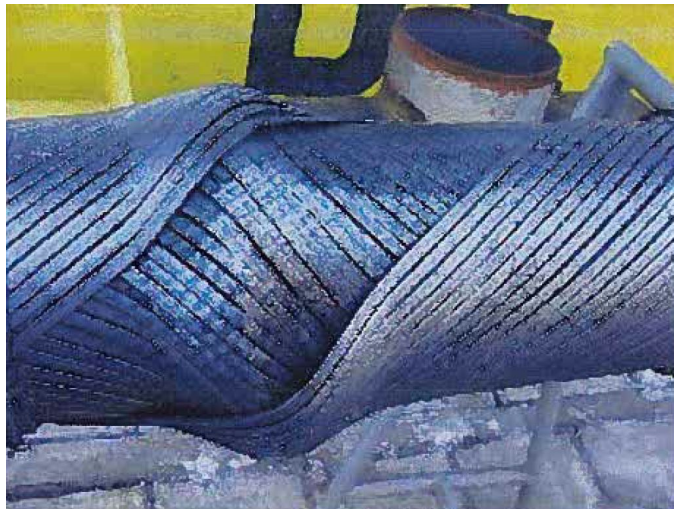

Figure 2.5: Example of bird caging of tensile armour wires [8].

The two main parameters governing bird caging are the loads on the pipe and the structure of the pipe. The dominating loads are pipe axial compression, pipe bending and the annulus condition. Bird caging is usually resisted by the external hydrodynamic pressure acting on the external sheath, but if the external sheath is damaged problems may arise. For the structure the inner diameter, tendon size, wire lay-angle, tape strength and interlayer friction are important parameters [15].

Solutions to prevent radial buckling is to avoid riser configurations that lead to excessive compression. If this is not possible additional support for the wires may be added by applying high strength tapes around the armour layers [1].

Bird caging may also occur from torsional failure if the acting forces are large enough. To avoid this either the torsional loads have to be reduced or the torsional capacity has to be increased by for example changing the lay angle of the wires or adding extra tensile armour wires [4].

2.4.2 Lateral buckling of tensile armour wires

If radial movement is sufficiently restrained, either by high strength tapes or sufficiently large external pressure, the tensile armour wires are forced to move laterally. This may result in lateral buckling as seen in figure 2.6.

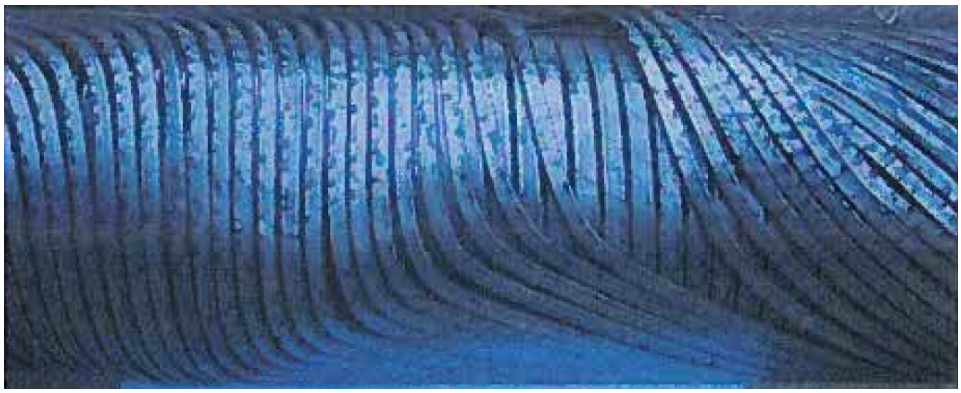

Figure 2.6: Example of lateral buckling of tensile armour wire [8].

As opposed to bird caging the lateral buckling of flexible pipe is difficult to detect since the deflection of the tendons is in the lateral direction and is covered by the external sheath. It is therefore important to be aware of the mechanisms triggering lateral buckling of the tensile armour wires when designing the flexible pipe.

Some mechanisms have been detected to cause lateral buckling. One mechanism is the reverse end cap effect. This is characterized by the flexible pipe having a very low internal pressure so that the hydrostatic pressure introduce very high compressive forces in the tensile armour wires. The effect is relevant especially under installation of the flexible pipe, but it may also be the case if the floating production unit is temporarily shut down [9].

Another mechanism found to cause lateral buckling is repeated bending cycles where the wires are moving sideways in a cyclic pattern. When the instability is reached the sideways motion is not symmetric any more and at the end of each cycle the wire position does not fully recover to that of the previous cycle. This effect increases at each bending cycle and may lead to global failure of the flexible pipe [2]

If the outer sheath is damaged the risk of lateral buckling increases. When the annulus is wetted the external pressure no longer causes contact stresses in the wires which would enable friction to limit wire slippage. This failure mode is governed by very large lateral deflections of the armour wires [9].

3 Literature survey

3.1 A finite element model for flexible pipe armour wire instability

Vaz and Rizzo [7] developed a non-linear static finite element model to simulate the flexible pipe armour structural instability and to predict the critical load and the morphology of the wires after instability. The model consisted of one wire representing the inner tensile layer and one wire representing the outer tensile layer, both resting on non-linear elastic springs. The wires were given geometric properties proportional to the number of wires in each layer. A cylindrical surface was placed between the layers to simulate the contact between them.

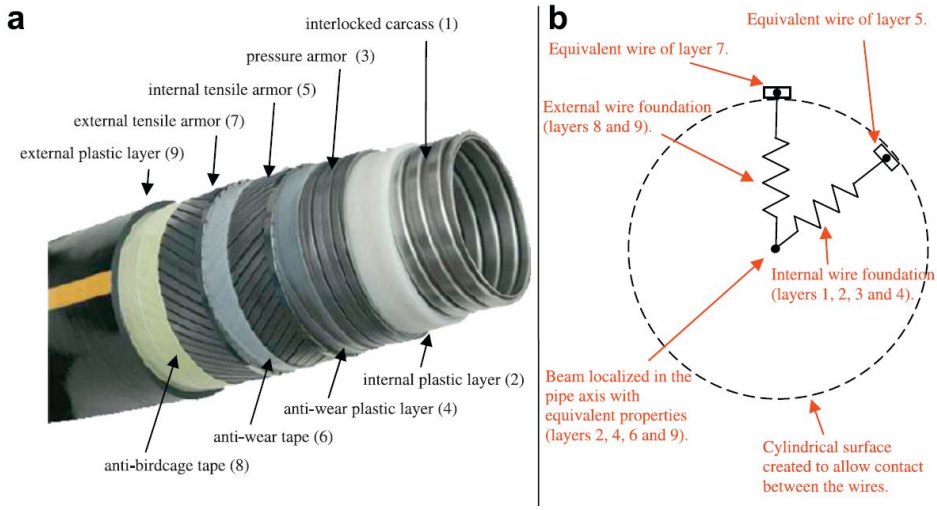

Figure 3.1: (a) Typical flexible pipe; (b) The proposed model [7].

The springs for the internal wire was modelled only to resist inward radial displacement, while the springs for the external wire was modelled only to provide strength against radial expansion. In addition a beam was placed in the pipe axis to represent the axial and torsional stiffness of the polymeric layers.

Loading was carried out in two steps. First the external pressure was applied on the cylindrical surface and secondly compression was applied to the wire ends. The pipe was loaded in this way to avoid localized bending near wire ends.

Since the structure would "dynamically" assume a new equilibrium configuration far from the initial condition "spurious" viscous damping forces were introduced into the global equilibrium equations.

A 9.5" flexible pipe with lay angle of 30^o and 74 armour wires in both internal and external tensile layers was used for the instability analysis. A rectangular cross section of 3 x 10 mm were used for the wires. The wire material was high strength carbon steel with yield stress 1100 MPa and rupture stress of 1500 MPa. The anti-birdcaging tape was set to a thickness of 2.4 mm, modulus of elasticity of 35 GPa and rupture stress of 261 MPa. The stiffness of layers 1-4 was set equal to $5\ x\ 10^6$ N/mm.

Parametric studies were performed with friction parameter between 0 and 0.4 and external pressure from 0 to 15 MPa. The instability load was taken as the maximum load supported by the structure when the displacements were imposed. When the wires instabilize the load suddenly drops.

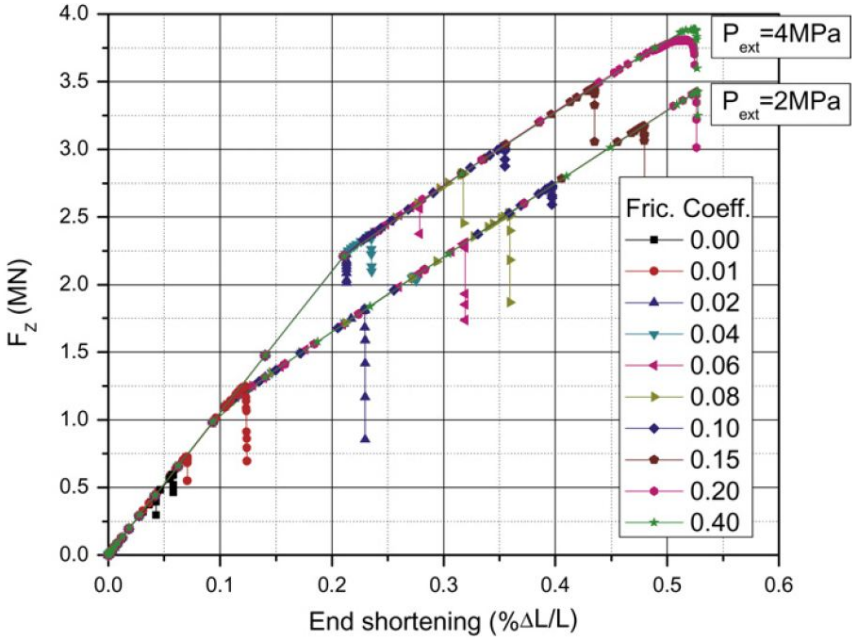

Figure 3.2: Compressive load versus end shortening [7].

A reduction of the inclination of the curves in Figure 3.2 were recorded. The change in stiffness occurred when the wires overcame the external pressure and could rest on the high strength tape. For an external pressure of 2 MPa this occurred when the end shortening was approximately 0.1%, while for external pressure of 4 MPa it occurred at 0.2%.

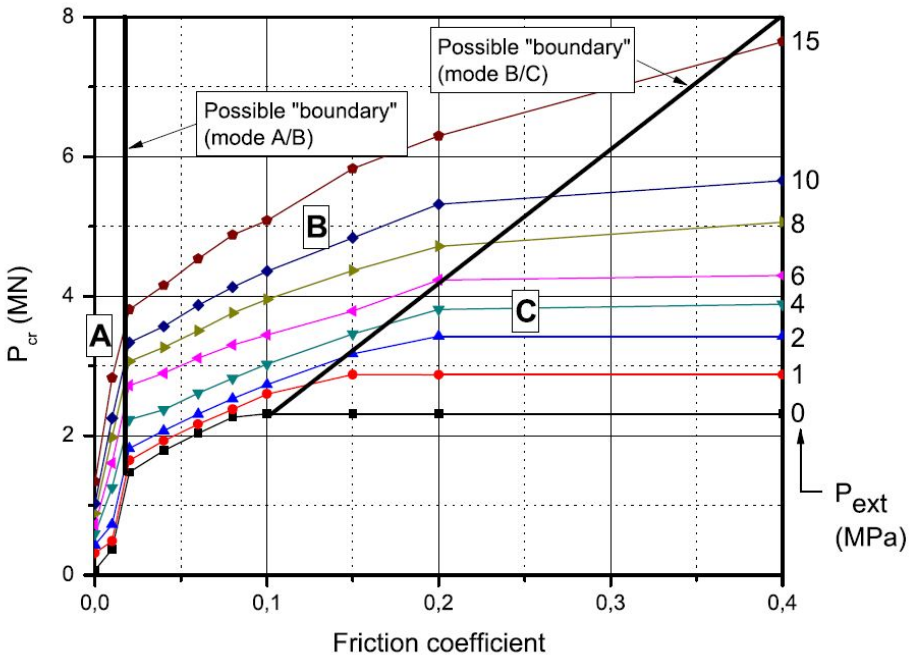

Figure 3.3: Instability load versus friction coefficient [7].

Depending on the friction coefficient and the external pressure applied four different types of instability modes were recorded:

- Mode A - lateral instability. Each equivalent wire instabilize independently.
- Mode B - lateral instability. The equivalent wires behave as a unique layer.
- Mode C - radial instability or birdcaging. The high strength tape has failed and the load is independent of the friction coefficient.
- Mode D - radial instability. Spatial buckling of armour wires. Observed for high friction and high pressure.

The most critical condition were experienced when the annular was flooded because the hydrostatic pressure did not support the wires and also a substantial reduction of the friction coefficient.

It should be mentioned that geometrical imperfections and residual stresses were not introduced in these studies. Introducing this would expectedly reduce the critical instability load.

3.2 On lateral buckling failure of armour wires in flexible pipes

In the paper by Oestegaard, Lyckeggaard and Andreasen in OMAE2011 [9] a model was proposed to predict the wire equilibrium state within the pipe wall and to predict lateral buckling. The model of the single wires were based on equilibrium of curved beams and the curvature expressions derived on basis of differential geometry. The following assumptions were made:

- Constant radius of curvature
- No friction
- Wire angle remains constant in outer layer (no transverse slip)
- No radial deformations due to axisymmetric loading

Assuming no transverse contact between the wires the complete model of the flexible pipe cross section was generated using the single wire model. Based on observations from experiments the inner tensile armour layer was considered free to seek equilibrium transversely. Effects from other layers were neglected. The tensile wires were considered isotropic and made of steel with elastic modulus 210 GPa and yield stress of 765 MPa.

Table 3.1: Tensile armour properties [9].

-	**Inner layer**	**Outer layer**
OD (m)	0.2012	0.209
L_{pitch}	1.263	1.318
Wire size (mm)	3 x 10	3 x 10
Number of wires	52	54

Theoretical studies were carried out and compared to experiments carried out on a flexible pipe with properties as given in table 3.1 and length of 5 meters. Two different radii of curvature were examined for the stiff pipe structure and one radii for the elastic pipe structure. All cases recorded a significant softening behaviour and this was considered as limit point buckling.

Both pipe curvature and effect of radial expansion seemed to have limited influence on the buckling loads for the theoretical model. When comparing the theoretical results with the experimental studies a key observation was made. The modelled wires failed immediately when critical loads were applied, while cyclic bending must be applied in the experiments to overcome frictional effects before failure. It was also observed that the radius of curvature had a large influence on the number of cycles needed to trigger failure by lateral buckling.

Two buckling mode shapes were observed both experimentally and by modelling. Buckling mode A with large wire gaps and buckling mode B corresponding to small gaps but large deviations from the initial helical angle as can be seen in figure 3.4.

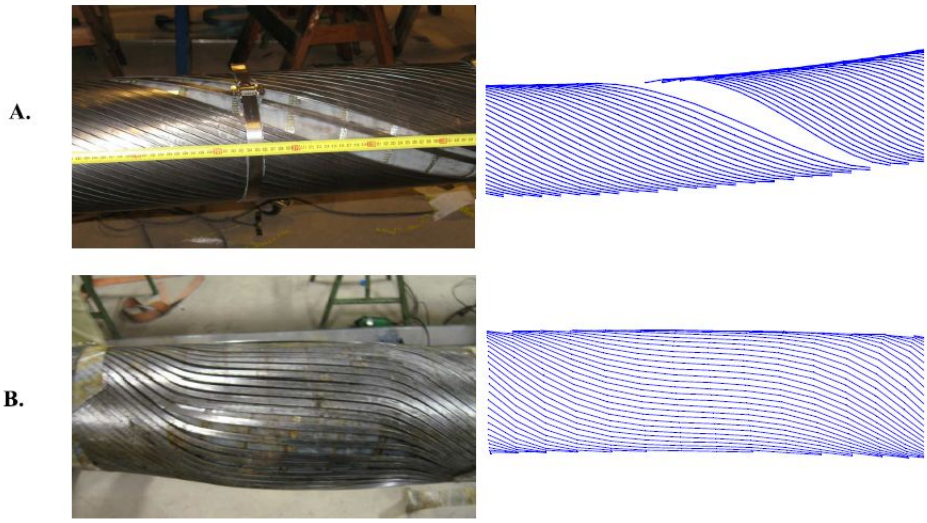

Figure 3.4: Detected buckling modes [9].

The calculated axial loads were also recorded. It was observed that setting the model length equal to the physical length of the test sample gives a conservative estimate for the limit buckling load. However friction and end fitting effects prevent the wires in the end of the pipe from slipping. To account for these non-slip zones the model length was set shorter than the physical length. Results showed that choosing a shorter length may impose severe impact on the buckling load.

4 Theory

4.1 BFLEX2010

The BFLEX2010 program is based on the principal of virtual displacements and the co-rotational formulation. Based on the work by Sævik [12] the number of degrees of freedom are minimised by neglecting transverse slip of the tensile armour wires thus resulting in the wires following a loxodromic surface curve as seen in figure 4.1.

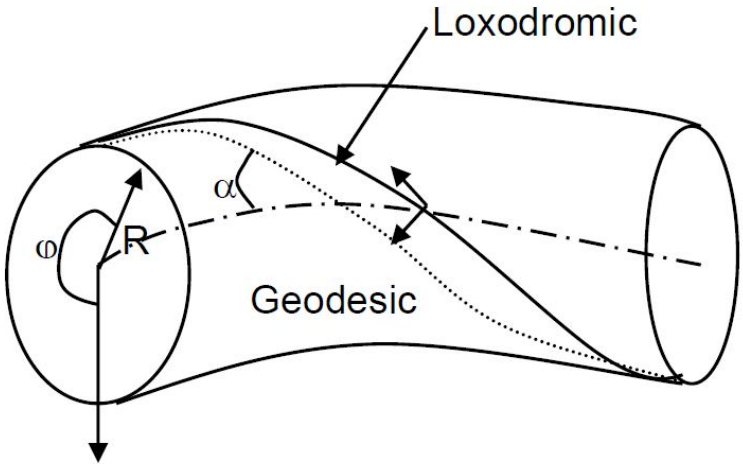

Figure 4.1: Loxodromic and geodesic curve along a curved cylinder [13].

For the tensile armour model the bending model can either be moment based or based on equilibrium considerations of each individual tendon. In this thesis the second approach is used and will be briefly presented in this section. For more details see the BFLEX2010 Theory Manual [13].

4.1.1 Pipe element

The pipe element used in this thesis is the "pipe31" element. This is a 12 degrees of freedom element used.

4.1.2 Spring element

For the springs used to represent the other layers of the flexible pipe and the loads applied the "spring137" element is used. The spring element consists of 12 degrees of freedom.

4.1.3 Sandwich beam theory

The Sandwich beam bending approach is formulated in terms of the potential energy of each wire.

$$\prod = \frac{1}{2}\int_0^l EA(\frac{du_s}{dX^1})^2 + \frac{1}{2}k(u_s - u_{1p})^2 dX^1 - Pv_{1p} \tag{4.1}$$

EA is the axial stiffness of the wire, u_s is the actual longitudinal displacement along the wire and u_{1p} is the wire displacement that would occur if plane surfaces remain plane after bending deformation. The shear deformation parameter γ and the shear stiffness parameter k are defined by [13].:

$$\gamma = \frac{v_s - v_p}{t} \tag{4.2}$$

$$k = \frac{Gb}{t} \tag{4.3}$$

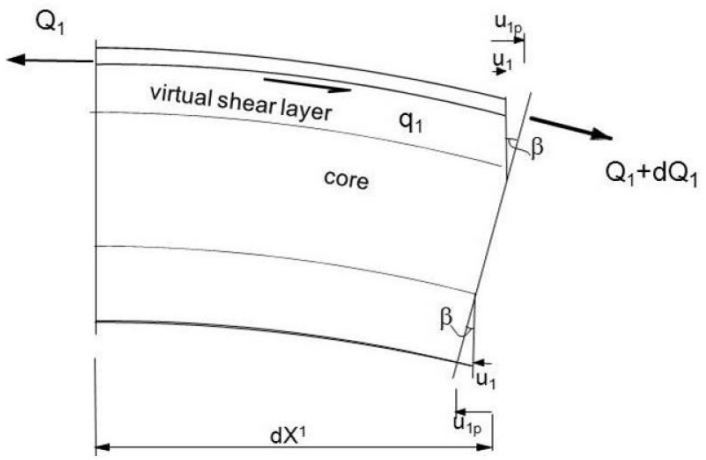

Figure 4.2: Shear interaction model for sandwich beam theory [13].

The deformation can be expressed by use of 3D-bream quantities if the wire surface is assumed to remain plain.

The friction model used consists of a friction surface and a slip rule and also accounts for material hardening [13].

4.1.4 Beam element

In order to also account for transverse slip, wire buckling and end fitting effects the new "hshear353" beam element has been introduced. The beam element uses the loxodromic curve as a reference curve from which arbitrary relative displacements are allowed to occur. For each wire the internal work contribution can now be described as:

$$W_i = \int_0^l [EA(\beta_{1,1} + u_{1p,1})\delta\beta_{,1} + GI_1(\omega_1 + \omega_{1p})\delta\omega_1 + EI_2(\omega_2 + \omega_{2p})\delta\omega_2 + EI_3(\omega_3 + \omega_{3p})\delta\omega_3 + \beta c\delta\beta]dX^1 \tag{4.4}$$

To capture buckling behaviour the coupling between global buckling and the different buckling failure modes about all axes of the wire has to be described. Also the prescribed kinematic terms from axi-symmetric response behaviour need to be included. The result is a 26 degrees of freedom beam element as seen in 4.3. The element allows for cubic interpolation in all directions thus avoiding the membrane locking phenomena due to the curvature coupling terms [11].

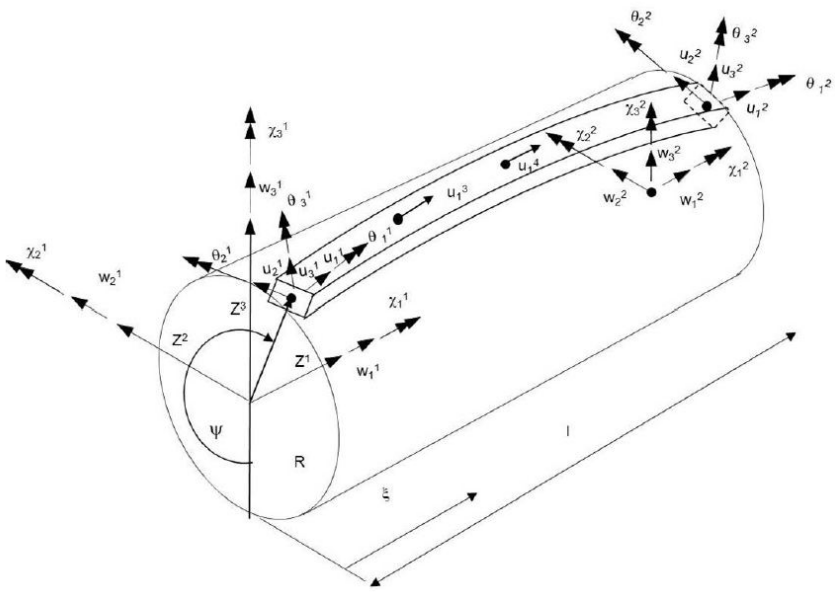

Figure 4.3: HSHEAR353 beam element [11]

4.1.5 Contact element

To describe the interaction between the layers the 24 degree of freedom contact element "hcont453" is used. This element is capable of describing the buckling process during cyclic loading by capturing the interaction between the layers. The interaction is described in terms of the interlayer contact forces and the friction related to relative displacements [11].

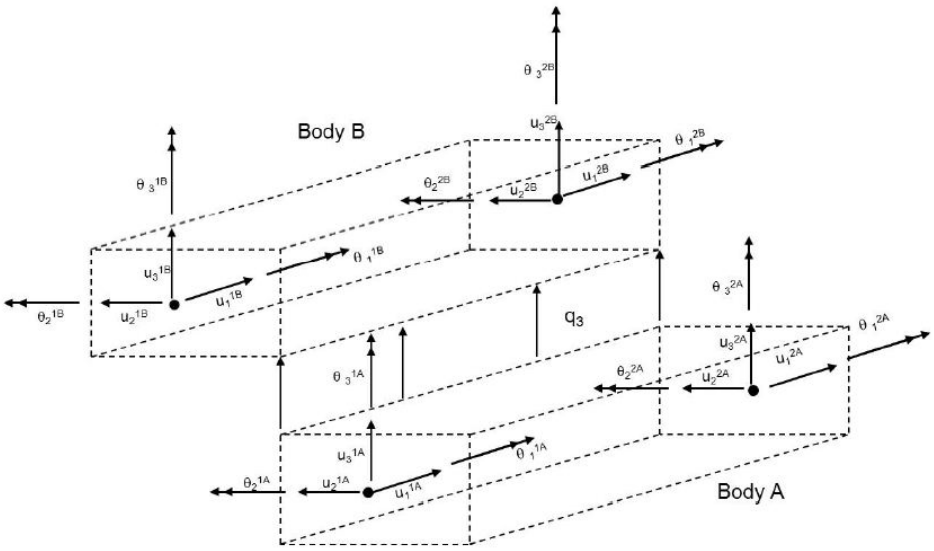

Figure 4.4: HCONT453 contact element [11].

Using this element enables the possibility to include linear varying line loads and still only have the displacements as unknowns in the FE equations. The "hcont453" finite element has the following key features:

- Describing the contact between layers of crossing tensile wires.
- Easily describe the resistance against wire rotation from other layers by including torsion coupling terms.

4.2 Analytical buckling methods

There is a close link between the friction force and buckling of the flexible pipe armour wires. This can be illustrated by looking at the reaction forces between the layers. A simplified model of the forces acting between the inner and outer wire can be seen in figure 4.5.

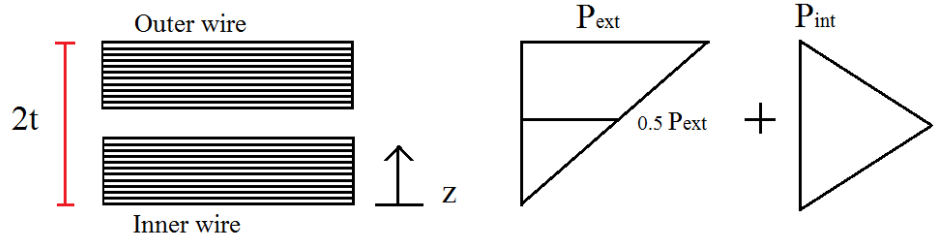

Figure 4.5: Simplified model of the force per unit length between the wires

The external reaction force is assumed to be half the external pressure between the wires. To find the internal reaction force we use the longitudinal strain for each wire obtained from pressure, tension and torsion loading.

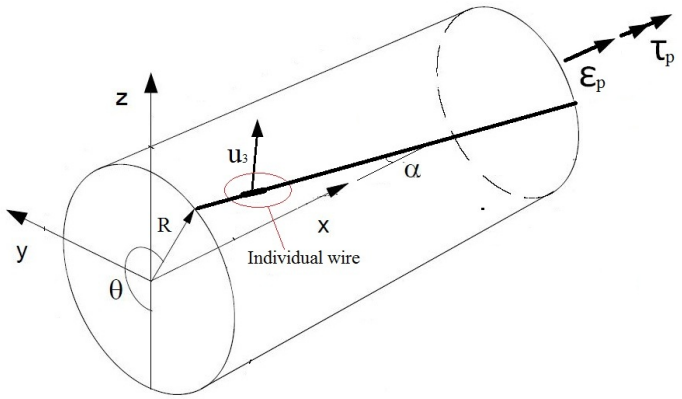

Figure 4.6: Simple model of pipe and tendon geometry

With reference to figure 4.6 the axial strain of each wire can be described by [13].

$$\epsilon_1 = \epsilon_p \cos^2 \alpha + \tau_p \sin \alpha \cos \alpha R + \frac{u_3}{R} sin^2 \alpha \tag{4.5}$$

Inserting this into the equations when calculating the stiffness matrix gives the internal reaction force.

$$P_{int} = EA \int_0^L \epsilon_1 \delta \epsilon_1 dx n_i \tag{4.6}$$

When this is known the available friction force between the wires can be expressed as:

$$\tau_f = \mu(P_{ext} + P_{int})\frac{b}{F_j} \tag{4.7}$$

To find the pre slip stiffness k_u

$$k_u = \frac{\tau_f}{\Delta} \tag{4.8}$$

The Δ symbol in this equation represents the pre slip distance. This is the distance the wires are allowed to slip before the friction factor starts acting.

When the pre slip stiffness is known we can calculate the value β_b used to find the buckling load. This is given by [14]:

$$\beta_b = \frac{k_u}{EI}(\frac{L}{\pi})^4 \tag{4.9}$$

The first buckling mode of the wire can be described by:

$$P_{m1} = P_E(1 + \beta_b) \tag{4.10}$$

The Euler buckling load is given by the following equation:

$$P_E = \frac{\pi^2 EI}{KL_k^2} \tag{4.11}$$

Varying the Δ value has a large impact on the buckling loads it is important to be aware of this when doing buckling calculations.

5 Creating the FEM-model

5.1 Main parameters

The FEM-model created is based on data given in the article by Vaz and Rizzo [7]. In the article a model of a 9.5" flexible pipe structure was created with 74 armour wires in the internal and external wire layd at an angle of 30 ° with respect to the pipe axis.

A 9.5" flexible pipe corresponds to 245.3 mm in diameter. In the article the internal and external radii are given to be 299.3 mm and 305.3 mm. It is assumed that the given numbers for helix radii in the article actually are the helix diameters. Thus the following key parameters are used in the model created in this thesis:

Table 5.1: Model data used for the model

Name	**Value**
Number of pitches	3
Lay angle of armour wire	30 °
Radius of inner armour wire	0.14965 m
Radius of outer armour wire	0.15265 m

With a laying angle of 30 degrees and 3 pitches the total length of the pipe can be found using simple trigonometry.

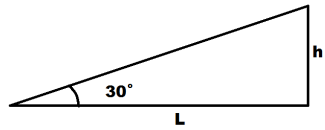

Figure 5.1: Calculating the length of the model

For three pitches the total height h will be 3 times the circumference of the pipe. Using the outer radius this gives the following length of the model:

$$L = \frac{6\pi R}{tan30°} = 4.9837\ [m] \tag{5.1}$$

Some other important assumptions for the model is that the acceleration of gravity and the mass proportional damping factor are set to zero. The stiffness proportional damping factor is set to 0.09 and an approach applying a consistent mass matrix is used. The analyses carried out is to be dynamic and the stress state at the start of the analyses are assumed to be stress free. The definition of axes is as defined in figure 4.6 with the x-axis along the pipe axis.

5.2 Tensile armour wires

The tendons are modelled with a rectangular cross section using the shearhelix theory [13]. For both the inner and the outer wire a scaling factor of 74 is used in order represent all the wires in each layer of the cross section and not just single wires.

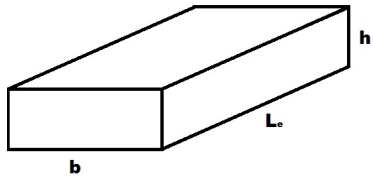

Figure 5.2: Simple model of the wire cross-section

In accordance with the model by Vaz [7] b is set to be 10 mm and h is to be 3 mm.

5.3 Number of elements

When selecting the number of elements it is important to consider the Euler buckling. The Euler buckling load is given by the following formula:

$$P_E = \frac{\pi^2 EI}{KL^2} \tag{5.2}$$

Assuming the wires to be pinned, but free to rotate, the factor K is set equal to 1. Also taking into account the scaling factor of 74 for the wires and that the wires are located with an angle of 30 ° compared to the pipe axis the following formula for the required element length can be used:

$$L_e = \sqrt{\frac{74\cos 30\pi^2 EI}{P_E}} \tag{5.3}$$

Since radial buckling is prevented we must find the moment of intertia about the strong axis. According to figure 5.2 the following formula can be used:

$$I = \frac{1}{12}hb^3 \tag{5.4}$$

We must also take into account that the tendons are oriented with an angle of 30 degrees compared to the circular pipe cross section. The critical element length is therefore decided by the following formula:

$$L_e = \sqrt{\frac{74cos(30)\pi^2 Ehb^3}{12Pcr}} \tag{5.5}$$

The only unknown in this equation is the buckling load P_{cr}. Looking at figure 8 in the article by Vaz [7] we can see that for the maximum external pressure of

15 MPa the maximum instability load recorded in the flexible pipe is just beneath 8 kN. To add extra safety a critical load of 10 kN is used to calculate the critical element length. Inserting data gives the following critical length for the wires:

$$L_e = 0.055\ [m] \tag{5.6}$$

To be sure to avoid local buckling of the tensile armour wires the total number of elements is chosen to be 200 corresponding to an element length of approximately 0.25 meters.

5.4 Nodes and boundary conditions

In order to create the flexible pipe cross section a total of 5 nodal point series are created. To easily distinguish the nodal points from each other they are numbered systematically as seen in table 5.2.

Table 5.2: Nodal point series with short description

Nodal numbers	**Description**
1 - 201	Nodal system along the pipe axis in the center of the pipe.
10 000 - 10201	Nodal system going helically around the pipe following the radius of the inner armour wire
20 000 - 20201	Nodal system going helically around the pipe in the opposite direction of the 10 000 series. Following the radius of the outer armour wire.
30 000 - 30201	Identical to the 10 000 series.
40 000 - 40201	Identical to the 20 000 series.
80 000 - 80201	Identical to the 20 000 series.

The difference between the nodal point series using the same coordinates is the boundary conditions. The 10 000 and 20 000 nodal point series are fixed in all six degrees of freedom and will stay at the exact same position at all times independent of what loading is applied. This is not the case for the 30 000 and 40 000 nodal points, which will always be in the center of the wires even when displacements are imposed. The 30 000 and 40 000 series are fixed from rotation about the x-axis and at the ends they are also fixed in the x and y direction. This means that the will follow the pipe core.

The pipe core is fixed from displacement in the y- and z-direction, and also fixed from rotating about the y- and z-axis. This means that the are free to move only along the x-axis along the pipe axis and to rotate about the x-axis if torsion is applied. In order to apply the end compression the middle node are fixed from both x-displacement and rotation about the x-axis.

The 80 000 nodal point series are fixed in all directions except movement in the z-direction allowing for the external pressure to be applied.

5.5 Elements

In order to capture the behaviour of the different layers in the flexible pipe cross section seven separate element series were created. The elements were numbered in a similar way as the nodes and can seen in figure 5.3 displaying the end of the pipe. The nodal numbers are presented using blue text while the element numbers are presented using red text.

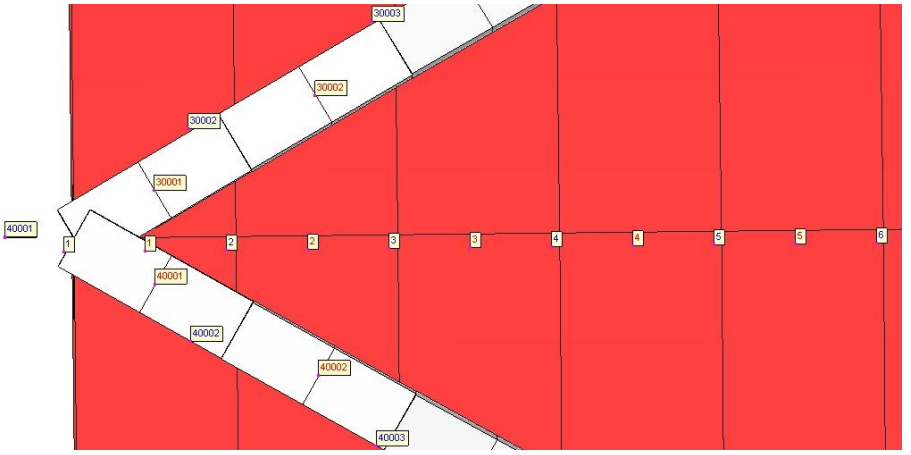

Figure 5.3: Example of the node and element numbers used for the model

The core of the pipe, the wires and the contact between the different layers are created using the elements described in chapter 4.

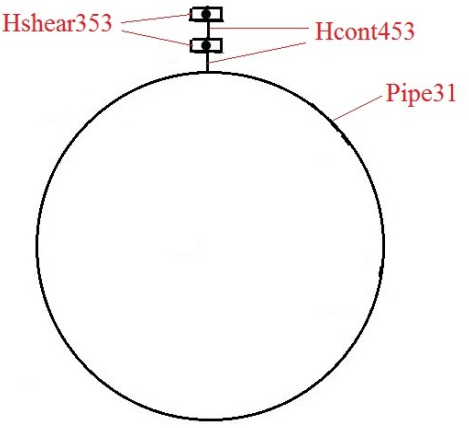

Figure 5.4: Simple model of the elements used to model the cross section

In figure 5.4 the core, wires and contact elements are indicated. To indicate how the springs are applied to represent the different layers of the cross section a

reference is made to the 20 000-, 40 000- and 80 000 nodal point series. Before loading these series are located at the exact same position.

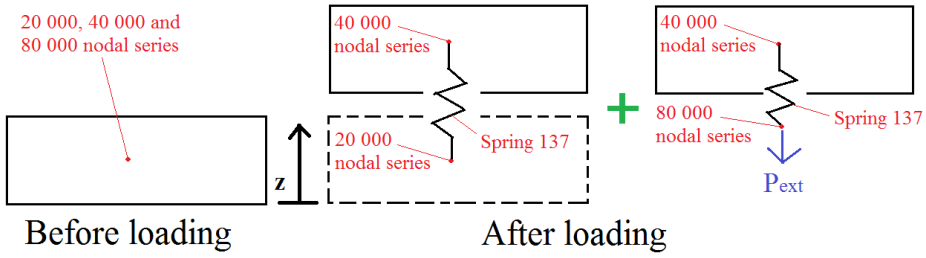

Figure 5.5: The spring elements before and after loading is applied

After loading is applied the outer wire will start to move. When this happens the spring between the nodal point of the 20 000 series and the 40 000 series will try to resist outward radial displacement. The external load is applied on the 80 000 nodal points, which again is connected to the 40 000 series by a spring. In this way the complicated flexible pipe cross section is modelled in a simple way.

A short summary of the numbering of the element series and the elements used can be found in table 5.3.

Table 5.3: Short description of the elements used for the model

Element type	**Numbering**	**Description**
Pipe	1-series	Pipe31 element defining the pipe wall.
Inner wire	30 000 series	Hshear353 element defining the inner wire.
Outer wire	40 000 series	Hshear353 element defining the outer wire.
Contact elements	50 000 series	Hcont453 element describing the contact between the pipe wall and the inner wire.
Springs	60 000 series	Spring137 element resisting the wire to move radially outwards.
Contact elements	70 000 series	Hcont453 element describing the contact between the inner and the outer wire.
Springs	80 000 series	Spring137 element used to apply the external pressure.

5.6 Loading

During the first 10 seconds of the analysis the dry mass is applied to the model. Then the loading is applied in the same manner as in the article by Vaz and Rizzo [7].

- The external pressure is applied between 10 and 20 seconds.
- End compression is added from 20 seconds and to the end of the analysis after 101 seconds.

In order to calculate the magnitude of the external pressure the total area of which the pressure acts must be found. This can be done using the radius of the outer wire and the following formula:

$$A_{pipe} = 2\pi R * L_{pipe} = 4.78m^2 \tag{5.7}$$

Using a reference pressure of 1 MPa gives the following force needed to represent the external pressure:

$$F_{pipe} = A_{pipe} * 1MPa = 4.78MN \tag{5.8}$$

When using 200 elements the force applied to each element will be 23.9 kN.

To apply the end compression a pre described displacement is added to the pipe ends. A reference displacement of 0.025 meters is applied to each of the ends.

5.7 Applying the external pressure

The external pressure is applied in three different ways. In the first case the load is applied by applying a force of 23.9 kN on each of the springs in the 80 000 nodal point series. These nodal points are connected by a spring to the 40 000 nodal point series representing the outer wire as described in figure 5.6. In this way the external pressure is acting on the outer wire.

In the second case the element connectivity of the spring is modified. This is done by connecting the 80 000 nodal points to the 30 000 nodal points representing the inner wire. Again the external pressure force is applied to the 80 000 nodal points, but now they are acting on the inner wire instead of the outer wire.

In the final case the 80 000 nodal point series are removed and the external pressure is applied to the model by imposing pre described displacement directly on the 20 000 nodal points on the springs representing the outer sheath. The 20 000 nodal series will now be free to move in the z-direction. The needed displacement to represent an external pressure force of 23.9 kN can be calculated from the following formula:

$$F_{spring} = k_{spring} u_{spring} \tag{5.9}$$

Since the stiffness k is not known the needed displacement must be found by trial and error. The displacement found to give a force of 23.9 kN was 0.0004906 meters.

5.8 Material

For the wires an elastic modulus of 210 GPa is used. For the pipe core the following values are specified:

- EA = 302 kN
- EI_y = 32.1 kN
- GI_t = 42.1 kN

5.9 Friction

For the springs between the 20 000 and 40 000 nodal points, and between the 40 000 and 80 000 nodal points Couloumb friction is applied. This means that the friction force in the x- and y-direction is multiplied with the force in the z-direction.

When applying the friction a slip distance must be defined. Before the slip distance is reached the model will act like a beam resting on an elastic surface.

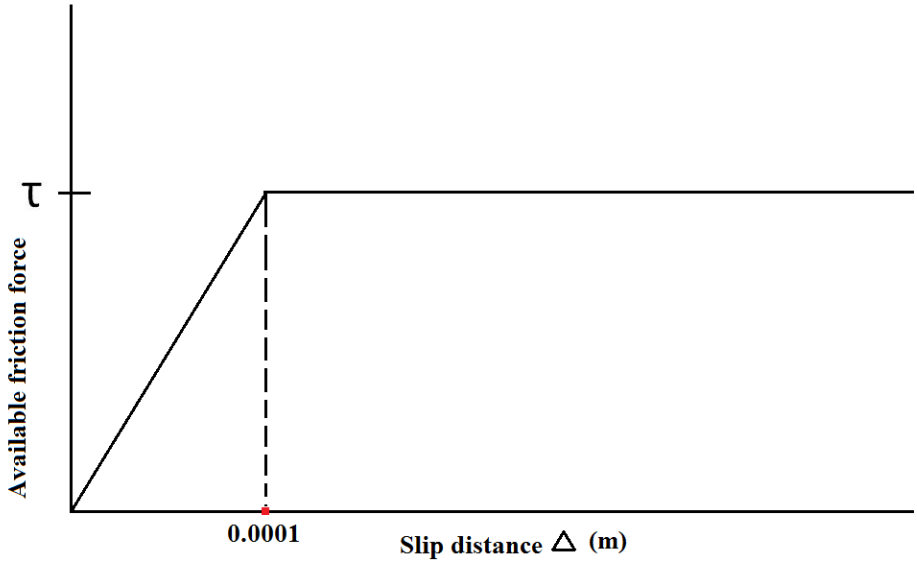

Figure 5.6: The spring elements before and after loading is applied

The slip distance specified in the model created is 1 mm.

All the details for the model are saved to the to BFLEX2010 input file. See appendix C.

6 The analysing process

In this chapter the most important software used for the analysis will be briefly presented. The emphasis will be on explaining the setup of the analyzing process and how the analyses are carried out using the different programs and input files.

6.1 Software

To carry out the analysis many different programs has been used, but the most important ones are the following:

Table 6.1: Software used for the analyses

Program name	**Description**
Matlab	Extensive mathematical program allowing for amongst other matrix operations, plotting of data, reading data from files and writing data to files. Licensed software.
Cygwin	Windows program with the possibility to use an environment similar to UNIX with built in gcc and bash compilator. Free software.
Bflex2010	Computer program performing the global and tensile armour analysis of flexible pipes. Marintek software.
Bflex2010post	Postprocessor for Bflex2010 exporting key results from analysis to file. Marintek software.
Xpost	Visual display of results from Bflex2010 analysis. Marintek software.
Matrixplot	Plotting of column oriented data related to structural engineering applications. Marintek software.

More detailed information about these programs can be found in their respective manuals.

6.2 Preparing the analyses

Manually varying the input parameters for each analysis carried out in this thesis would require a lot of time. To avoid this unnecessary use of time a more automatic approach allowing for multiple analysis being carried out automatically were created. The following files were created for this purpose:

- inputwriter.m: Matlab script to define and vary input parameters and create the go-analyze script.
- go-analyze: Perl script to be executed in Cygwin allowing for multiple analyses using Bflex2010 with different input parameters.

- go-plot: Perl script used by go-analyze script to generate plots of the results.

The first step of the analyzing process would be to create an empty folder containing these files. In addition the following files must be copied to the same destination:

- vazv2_1.2bif: The input file for the Bflex2010 analysis.
- mplot_oc.2bpi: The input file for Bflex2010post to generate the result files.

These files can be found in Appendix A through Appendix E.

6.3 Creating the input files

The second step is defining the input parameters and how these are to be varied throughout the analyses. This is done using the Matlab-script inputwriter.m. The following variables must be defined:

Table 6.2: Input parameters for the analysis

Input parameter	**Description**
Number of analyses	Total number of analyses to be run. Default value 1. If another value than 1 is specified the friction and external pressure will be varied according to table 8.2.
Friction	Friction factor applied for single analysis.
External pressure	External pressure applied for single analysis.
Stiffness scaling	Factor to modify the stiffness of the springs in the model. Default value 1.
Displacement scaling	Factor to modify predescribed displacements imposed on pipe. Default value 1.
Vaz variation	Parameter used to vary friction and external pressure according to Vaz [7]. Default value 1.

When these variables have been determined the script can be executed in Matlab. This automatically enters the parameters into the "go-analyze" file.

6.4 Executing the analyses

To start analysing the "go-analyze" file must be executed in the command window of Cygwin when located in the same folder as the file. The input parameters defined earlier are now automatically implemented into the Bflex2010 input file "vazv2_1.2bif". This is done by automatically replacing # followed by a certain textstring in the input file.

When the textstrings has been replaced by input parameters the analysis starts automatically using Bflex2010. The analyses will be executed one by one and

Before inserting input values

```
256 # External pressure
257 #        history number     time     loadfactor
258  THIST_R 400    0            10.0 rampcos 0.0
259              10.0           20.0 #pext
```

After inserting input values

```
256 # External pressure
257 #        history number     time     loadfactor
258  THIST_R 400    0            10.0 rampcos 0.0
259              10.0           20.0 rampcos 2
```

Figure 6.1: Example of how the external pressure is added to input file

the progress of each analysis can be monitored in the Cygwin window. Multiple windows running different "go-analyze" files can be executed at the same time if the computer used has sufficient capacity .

When running "go-analyze" the resulting files are systematically stored in different folders for each analysis. All analyses will be added to the main folder containing information about time, date of the analyses and a short description. New sub folders will be created for each analysis. The folder name for each analysis contains the number of the analysis, the friction coefficient used and also the external pressure applied.

Folder

Name	Date modified
Analyse_2012_5_22_18_11_NewElements_1	22.05.2012 19:41
Analyse_2012_5_23_10_32_ChangedBC_1	23.05.2012 10:40
go-analyze	23.05.2012 10:33
go-plot	18.05.2012 18:06
inputwriter.m	23.05.2012 23:19
mplot_oc.2bpi	22.05.2012 17:58
vazv2_1.2bif	22.05.2012 18:00

Subfolder

Name	Date modified
Analyse1_fric=0_pekst=2	22.05.2012 18:28
Analyse2_fric=1.000000e-02_pekst=2	22.05.2012 18:35
Analyse3_fric=2.000000e-02_pekst=2	22.05.2012 18:43
Analyse4_fric=4.000000e-02_pekst=2	22.05.2012 18:48
Analyse5_fric=6.000000e-02_pekst=2	22.05.2012 18:53
Analyse6_fric=8.000000e-02_pekst=2	22.05.2012 18:59
Analyse7_fric=1.000000e-01_pekst=2	22.05.2012 19:06
Analyse8_fric=1.500000e-01_pekst=2	22.05.2012 19:19
Analyse9_fric=2.000000e-01_pekst=2	22.05.2012 19:32
Analyse10_fric=4.000000e-01_pekst=2	22.05.2012 19:41

Figure 6.2: Example of the folder system automatically created when executing the analyses

In addition all the files generated from running BFLEX2010post are placed in a separate folder named "matrixplots_original" for each analysis.

6.5 Viewing the results

To view the results of the analysis the programs Xpost and Matrixplots are used. In each analysis carried out a result file is created and this can be opened in Xpost for visualisation of the model. Xpost has several possibilities on how to view the model. Especially useful are the possibility to see the displacements of the different elements in the model for each time step. The displacement scaling factor can also be useful when trying to determine how the tensile armour wires buckle.

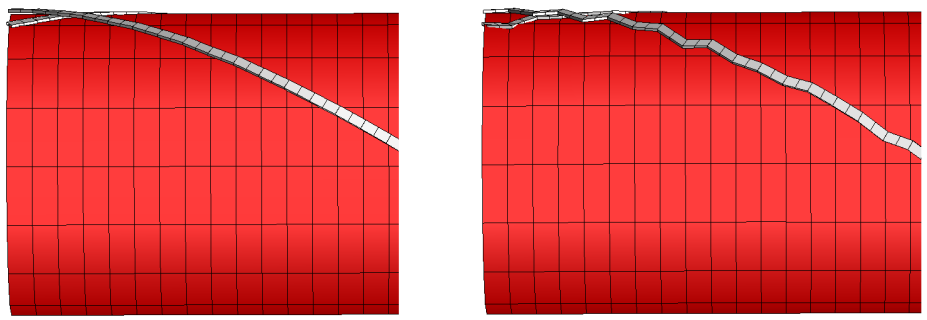

Figure 6.3: Example of the displacement of the model with and without displacement scaling

In figure 6.3 a visulazation of the model at the last time step prior to buckling is collected from Xpost. In order to get a better view of the displacement of the wires a displacement scaling factor of 10 is applied.

In order to view for example how the forces and displacements of the different layers vary with time the files created with Bflex2010post during the analyses can be viewed in Matrixplots. Some important graphs generated are:

- Time versus force in pipe wall
- Time versus force in inner wire
- Time versus force in outer wire
- Time versus end shortening in pipe wall
- Number of pitches versus angle between wire and pipe axis for inner and outer wire

To compare multiple analyses Matrixplots also has the ability to plot several curves in the same chart.

6.6 Determining the time of buckling

The armouring tendon wires are assumed to buckle either when there is a clear drop in the time versus force graph or if the analysis automatically stops before the final time step. An example can be seen in figure 6.4 where the blue line displays the classical drop in force and the black line displays that the analysis stops at time step number 63 out of 101.

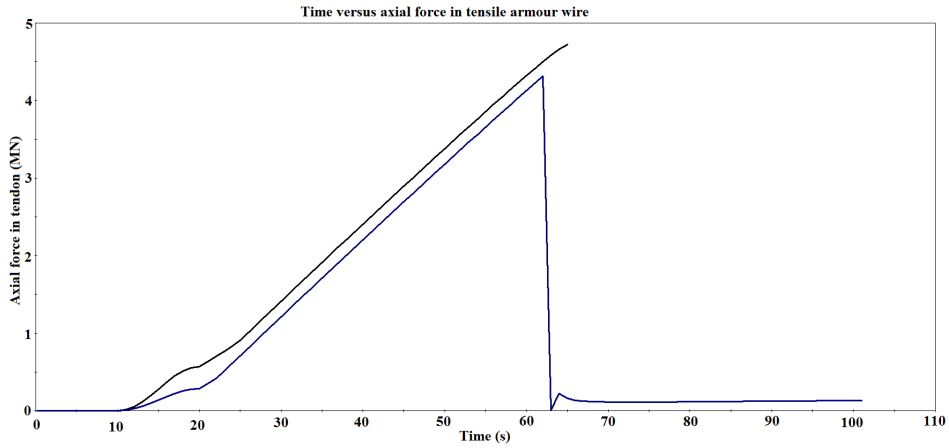

Figure 6.4: Using the 3D-mesh to check if buckling has occurred

From the curves the time of buckling is noted. Then the 3D-mesh of the model is used to confirm if buckling actually has occurred. This is done by checking the model at the time right before and right after buckling. An example of this can be seen in figure 6.5.

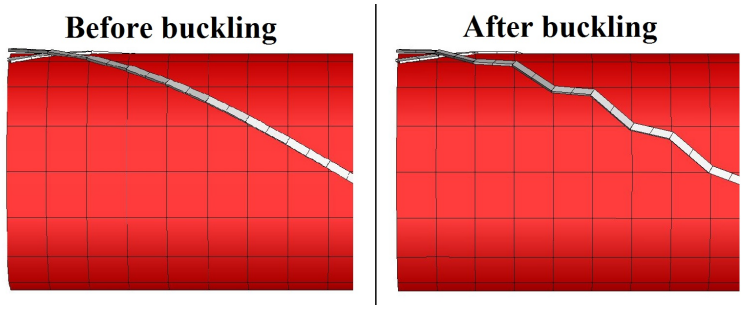

Figure 6.5: Deciding the onset of buckling

If the analysis is stopped before the final time step it is not able to view the model after buckling has occurred. An indication of whether buckling has occurred or not can however be found by checking the plots of pitch versus angle between the wire and pipe axis, θ_z.

6.7 Comparing multiple buckling graphs

When comparing multiple buckling graphs it may be difficult to distinguish the different curves. To make it easier to compare the graphs some small modifications are made.

- At the time of buckling the graph is cut off and a short vertical line is added indicating that buckling has occurred.
- Different colors and symbols are used for each case to distinguish between the different friction factors used.

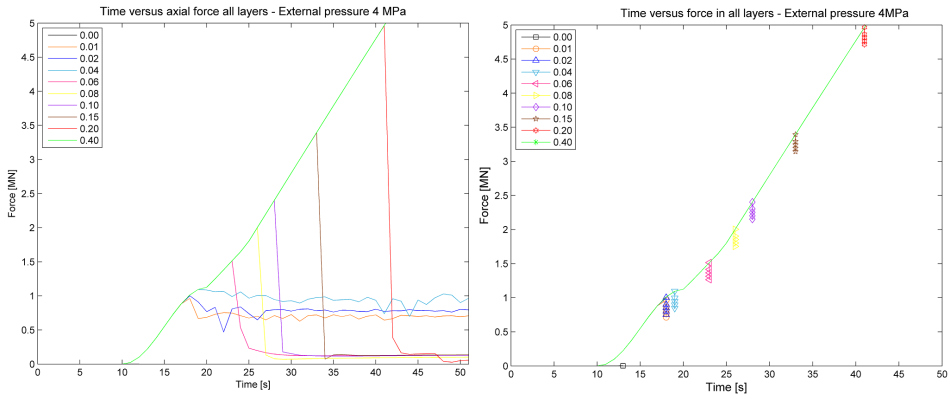

Figure 6.6: Time versus force graph before and after modification.

In figure 6.6 an example of a time versus force graph before and after modification can be seen. The symbols used for the different friction factors are created similar to the symbols used in figure 3.2.

A drawback of the Matrixplots program is that the graphs from each analysis must be opened manually in a one by one manner. In order to create multiple graphs, like the ones in figure 6.6, a Matlabscript named "amultiscan.m" was created. The script has the possibility to read the information from multiple analysis and plotting the results in the same graph by only specifying the folders of the result files. In the script it is also possible to determine which quantity is to be plotted at the x-axis and y-axis, opening for the possibility to generate plots of for example end-shortening versus force.

6.8 Generating the end shortening vs force curve

In order to compare the results from the analyses with the results in the article by Vaz and Rizzo [7] the corresponding end shortening must be determined. To get the end shortening of the armour wires in the same way as in figure 3.2 some modifications must be made. To do this we use the time versus strain graph for the pipe core.

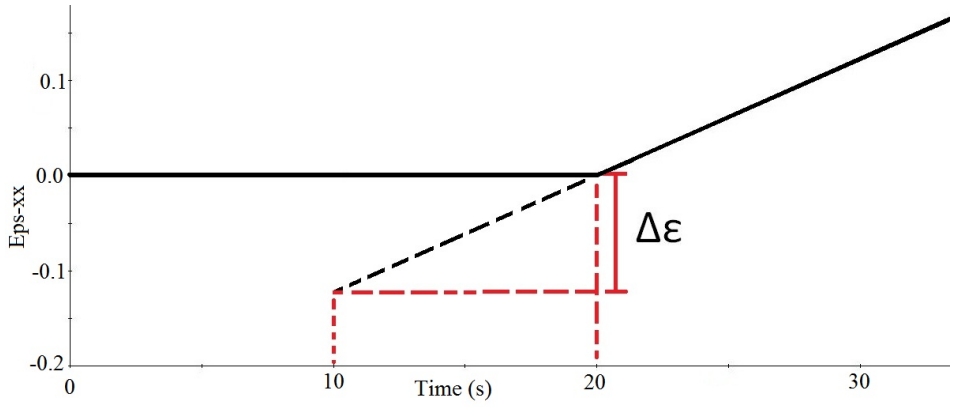

Figure 6.7: Extrapolation of the displacement curve

Even though the external pressure is applied between 10 and 20 seconds the strain is approximately zero. Strain is not evident in the curve until the end compression is applied after 20 seconds . By extrapolating the curve between 20 and 30 seconds the change in strain for a 10 second interval can be found. By using this value the force versus strain curve can be "shifted" to the left and the inclination can start after 10 seconds. The reason for doing this is to get curves like the ones in figure 3.2 where both force and end displacement are zero at beginning.

To correct for the change in force between 10 and 20 seconds the graph of the force in the wires are used. As seen from the graph the inclination of the time-force curve is steeper after 20 seconds when compared to the inclination prior to 10 seconds. This effect must also be incorporated into the modified time versus strain curve.

Denoting the change in force between 10 and 20 seconds ΔF_{10-20} and the change from 20 to 30 seconds for ΔF_{20-30} we can use the following formula for the change in displacement for the armour wire between 10 and 20 seconds.

$$\Delta\epsilon_{20} = \frac{\Delta\epsilon}{\Delta F_{20-30}} \Delta F_{10-20} \tag{6.1}$$

The modified strain in the tensile armour wires prior to 20 seconds can now be expressed as:

$$\epsilon_{10-19}(t) = \epsilon(t) + \Delta\epsilon_{20} \frac{t-10}{10} \tag{6.2}$$

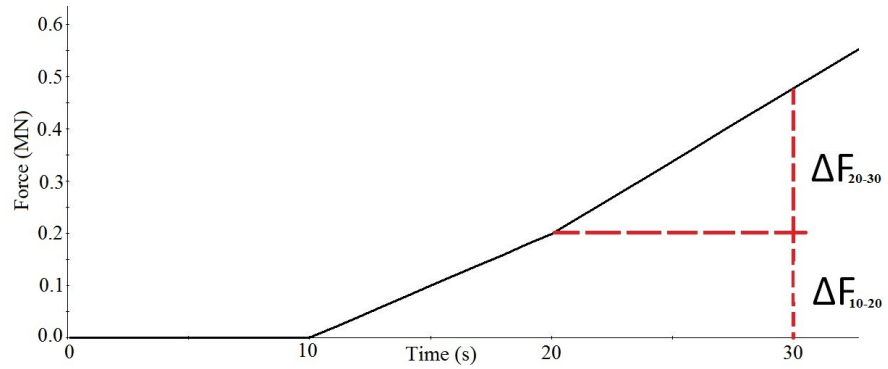

Figure 6.8: Extrapolation of the force curve

The modified strain after 20 seconds is given by:

$$\epsilon_{20-101} = \epsilon + \Delta\epsilon_{20} \tag{6.3}$$

This modification is done automatically using the "amultiscan.m" script . The modified time versus strain curve can be seen in figure 6.9.

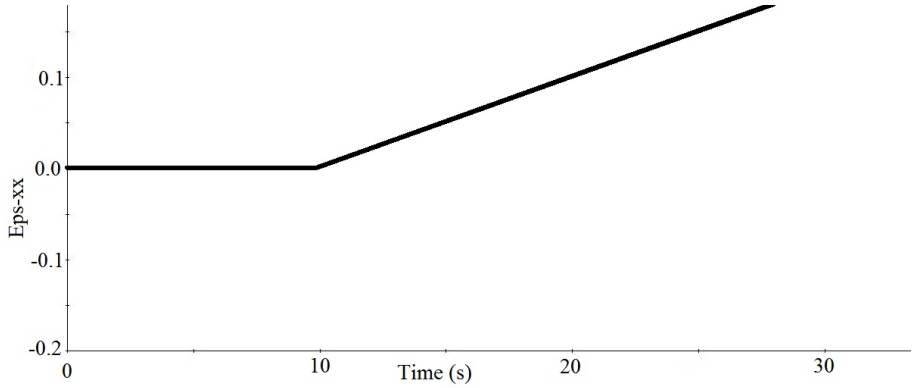

Figure 6.9: Extrapolation of the displacement curve

The Matlabscript "amultiscan.m" can be found in Appendix F.

7 Modelling sensitivity analyses

When doing analyses of the flexible pipe armour wires a lot of parameters must be defined and varied. To vary all of them would lead to a significant amount of different scenarios. In order to reduce the number of scenarios to a certain extent some sensitivity analyses were performed to study the effect of some key parameters on the results.

7.1 Time interval for applying the external load

As described in chapter 5.6 the external pressure is applied during the between 10 and 20 seconds of the analysis, while the compression to the ends are applied during the next 80 seconds. For low friction factors and external pressure above 4 MPa it was observed that buckling occurred while applying the external pressure.

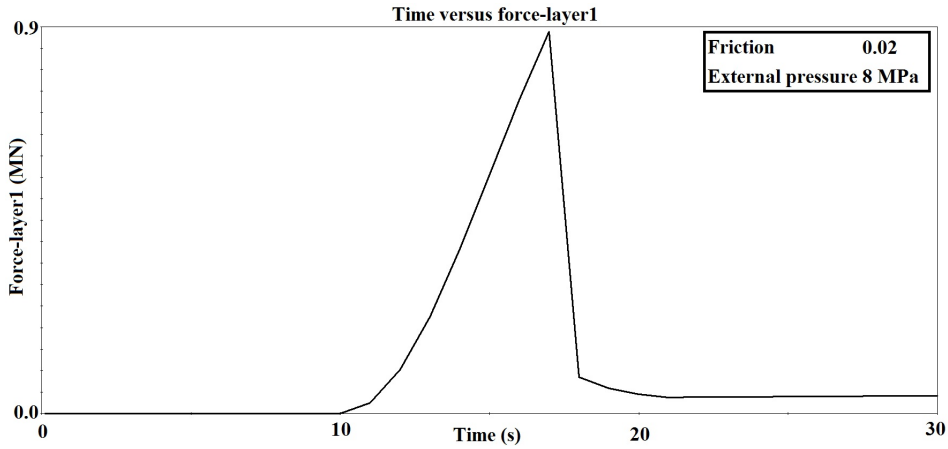

Figure 7.1: Time versus force using original time interval

As seen in figure 7.1 buckling of the armour wires occur after 17 seconds using an external pressure of 8 MPa and a friction factor of 0.02.

In order to investigate if the buckling observed was a result of the short time interval in which the external loading is applied some changes were made. The time interval for applying the external load was increased so that the load is applied between 10 and 60 seconds. A new analysis were executed with the exact same input data but using the new time interval.

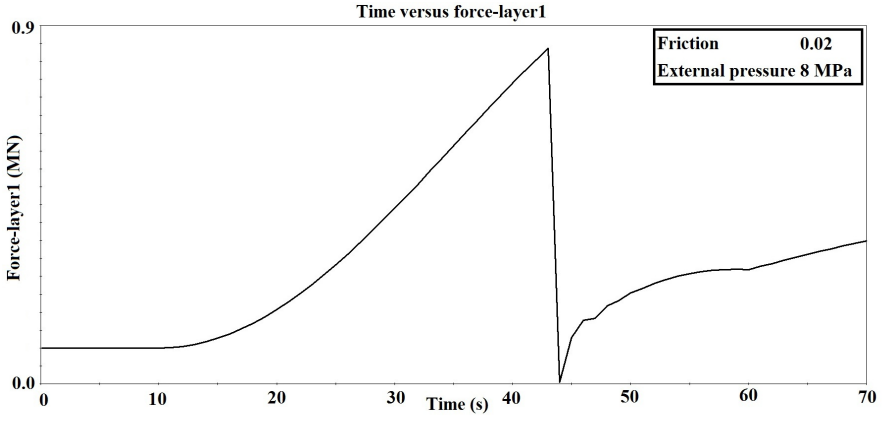

Figure 7.2: Time versus force using the new time interval

From figure 7.2 we can see that for an external pressure of 8 MPa and a friction factor of 0.02 buckling now occurred after approximately 43 seconds. The external load was not activated until 60 seconds. This indicates that the original time interval where the external pressure is applied during a 10 second interval is valid.

Table 7.1: Comparing time of buckling for original versus new time interval

Ext. pressure	**Friction**	**Original time**	**New time**
6 MPa	0.02	19	54
8 MPa	0.01	15	36
10 MPa	0.06	19	47
15 MPa	0.04	16	38

To rule out the possibility of this being a single happen stance a batch of analyses were carried out with the new time interval using different pressure and friction factors. The results can be seen in table 7.3. Since buckling occurred before the compression were initiated for all these cases it is assumed that the original time interval where the external pressure is applied between 10 and 20 seconds is valid.

7.2 Number of elements

In order to check if the number of elements affect the buckling load tests are carried out using both 100, 200 and 400 elements. In addition to increasing the number of nodes and the connected elements some other small changes must be made in the input file. These changes can be seen in table

Table 7.2: Modified input data for different number of elements

Number of elements	External pressure per node	Spring stiffness
100 elements	47.80 kN	$172 * 10^{11}$ N
200 elements	23.90 kN	$86 * 10^{11}$ N
400 elements	11.95 kN	$43 * 10^{11}$ N

Tests were carried out using different external pressures and friction factors. For the case using an external pressure of 2 MPa and friction factor of 0.2 the graph in figure 7.3 was obtained.

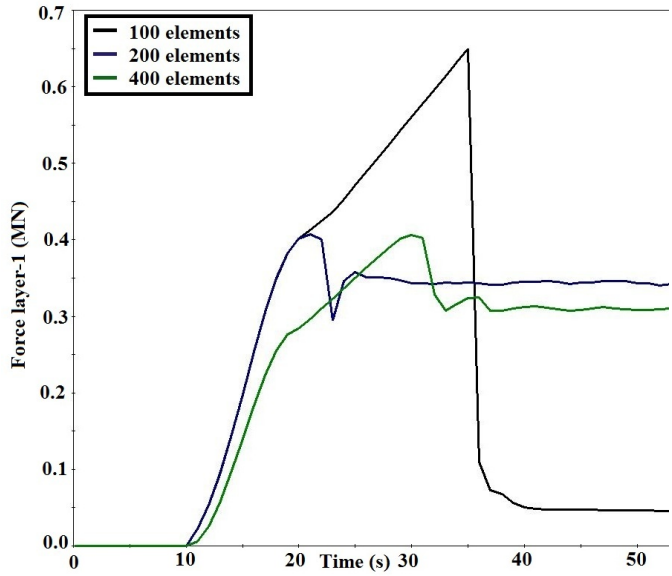

Figure 7.3: Comparison of buckling load for 100, 200 and 400 elements

As we can see in figure 7.3 the case using 100 elements results in a buckling load more than 60% larger than the cases using 200 and 400 elements. It can also be seen that the buckling loads using 200 and 400 elements results in approximately the same buckling load, but not at the same time. This may indicate that using 100 elements results in element lengths too close to the critical buckling length of the elements.

A case using an external pressure of 4 MPa and a friction factor is also carried out to control that the results in figure 7.3 were not a happenstance.

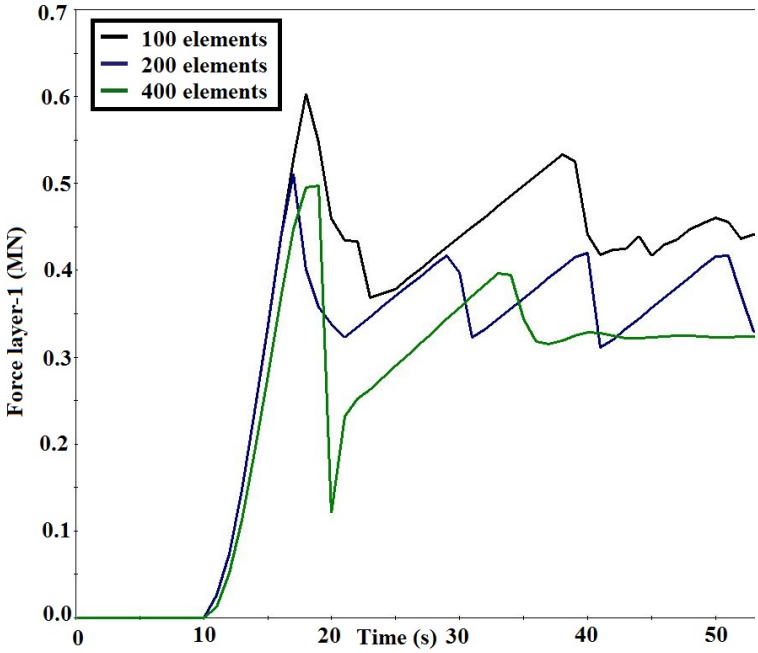

Figure 7.4: Comparison of buckling load for 100, 200 and 400 elements

As we can see from figure 7.4 the buckling loads for 200 and 400 elements are approximately the same, while the buckling load for 100 elements are approximately 20% higher.

From these results the assumption is made that using 200 elements should be sufficient when running the analyses.

7.3 Pre-described displacement

For the highest friction factors it may be the case that the wires do not buckle when imposing the pre described displacement. In order to ensure that all cases studied experience buckling analyses were performed where the magnitude of the pre described displacement were increased from the original 0.025 meters to 0.125 meters.

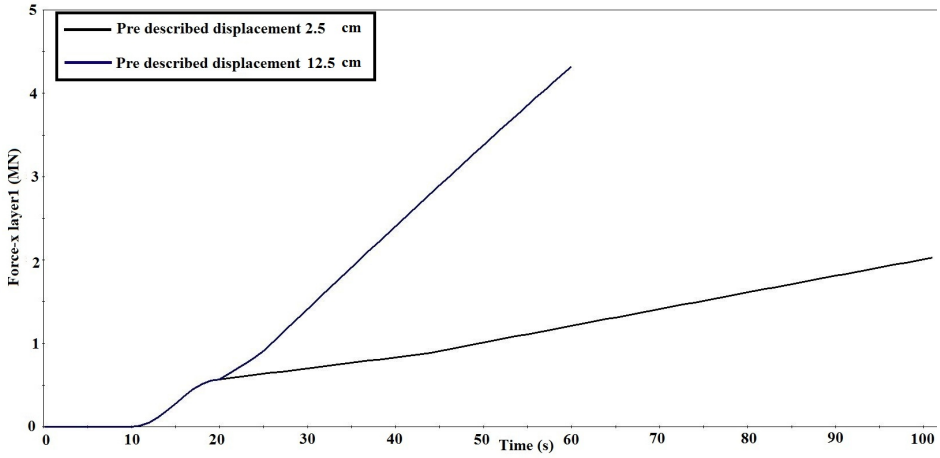

Figure 7.5: Comparison of buckling load for 100, 200 and 400 elements

In figure 7.5 en external pressure of 15 MPa and a friction factor of 0.4 is applied. As we can see in the case with a pre described displacement of 0.025 meters the wires do not experience buckling. When increasing the pre described to 0.125 meters the wires buckle after approximately 60 seconds. In order to ensure that increasing the pre described displacement does not affect the end-shortening versus buckling load curves we also have to investigate the time versus end shortening curve.

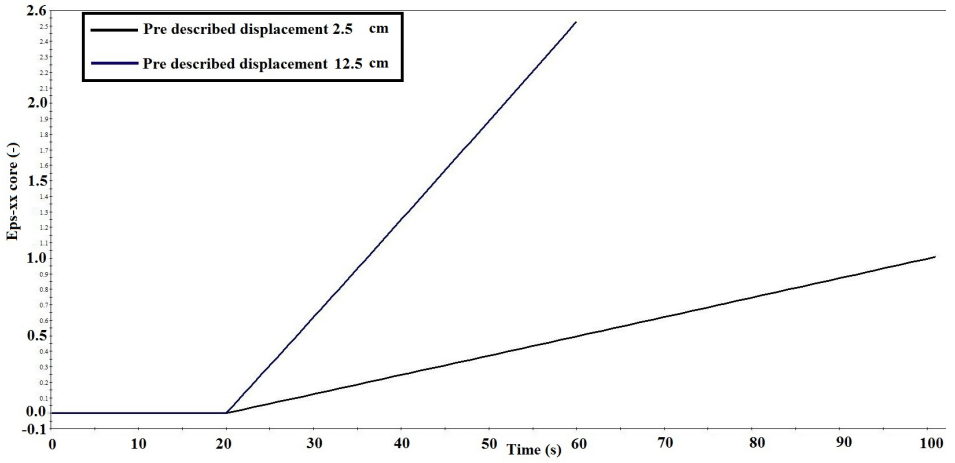

Figure 7.6: Comparison of buckling load for 100, 200 and 400 elements

As seen from figure 7.5 and figure 7.6 the graphs are exactly the same as the dry mass and external pressure are applied during the first 20 seconds. After 20 seconds the graph using a pre described displacement of 0.125 meters have an inclination approximately 5 times that of the graph using 0.025 meters pre described displacement.

To compare the values of the resulting cases the graph we would expect that the values after 30 seconds when the pre described displacement is 0.125 meters would be the same as the values after 70 seconds when the pre described displacement is 0.025 meters.

Table 7.3: Comparing force and end shortening for different pre described displacements

Pre described displacement	0.025 meters	0.125 meters
Time (s)	70	30
Force (kN)	1.41212	1.41223
End shortening ($\%\frac{\Delta L}{L}$)	0.62806	0.62806

As we can see the values are exactly the same for the end shortening and the difference in the forces of 0.00011 kN is negligable. It is therefore assumed that using a pre described displacement of 0.125 meters does not affect the results. It is also assumed that using this pre described displacement also ensures that buckling occur in all the cases studied.

8 Results

The model used for the analyses has been created according to the information given in the article by Vaz and Rizzo [7] as described in chapter 5. It is emphasized that not all information needed to recreate the exact same model was given in the article. For the information not given assumptions were made based on engineering judgements and discussions with professor Svein Sævik.

The analyses has been divided into separate cases depending on how the external pressure is applied and if the pipe is restrained from torsion or not.

Table 8.1: Short description of the six different cases studied.

Name	**External pressure applied as:**	**Torsion**
Case 1	Nodal point loads on outer wire	Allowed
Case 2	Nodal point loads on inner wire	Allowed
Case 3	Pre described displacement on outer wire	Allowed
Case 4	Nodal point loads on outer wire	Not allowed
Case 5	Nodal point loads on inner wire	Not allowed
Case 6	Pre described displacement on outer wire	Not allowed

As seen in table 8.1 a total of six different cases are analysed.

The main focus of this thesis has been to try to recreate the results in the article by Vaz and Rizzo [7] as seen in figure 3.2. For each of the six cases studied the combinations of external pressures and friction factors was varied accourding to table 8.2.

Table 8.2: Variation of the external pressures and friction factors in the analyses.

External pressure	**Friction factor**									
2 MPa	0.00	0.01	0.02	0.04	0.06	0.08	0.10	0.15	0.20	0.40
4 MPa	0.00	0.01	0.02	0.04	0.06	0.08	0.10	0.15	0.20	0.40

For each case the corresponding buckling modes are investigated by use of the 3D model and plots of the wire angle θ_z. Comparisons are made between the three first cases to investigate if the different ways to apply the external pressures has influenced the results. Comparisons are also made between the cases where torsion is allowed and where it is restrained.

Some analyses were also carried out where the models used in the cases in table 8.1 were exposed to external pressure ranging from 2 MPa to 15 MPa in order to investigate if the larger pressures led to larger buckling loads. The variations of external pressures and friction factors used can be found in 8.2.

Table 8.3: Variation of the external pressures and friction factors in the analyses.

Friction factor	**External pressure**					
0.40	2 MPa	4 MPa	6 MPa	8 MPa	10 MPa	15 MPa

Comparisons were also made between the different cases and the results obtained in the article by Vaz and Rizzo.

Finally some analyses are carried out where the slip distance is varied in order to see how this affect the buckling loads.

8.1 Case 1

When the external pressure is applied as nodal loads acting on springs connected to the outer tensile armour wire the following figure is obtained when using the procedure described in chapter 6.8.

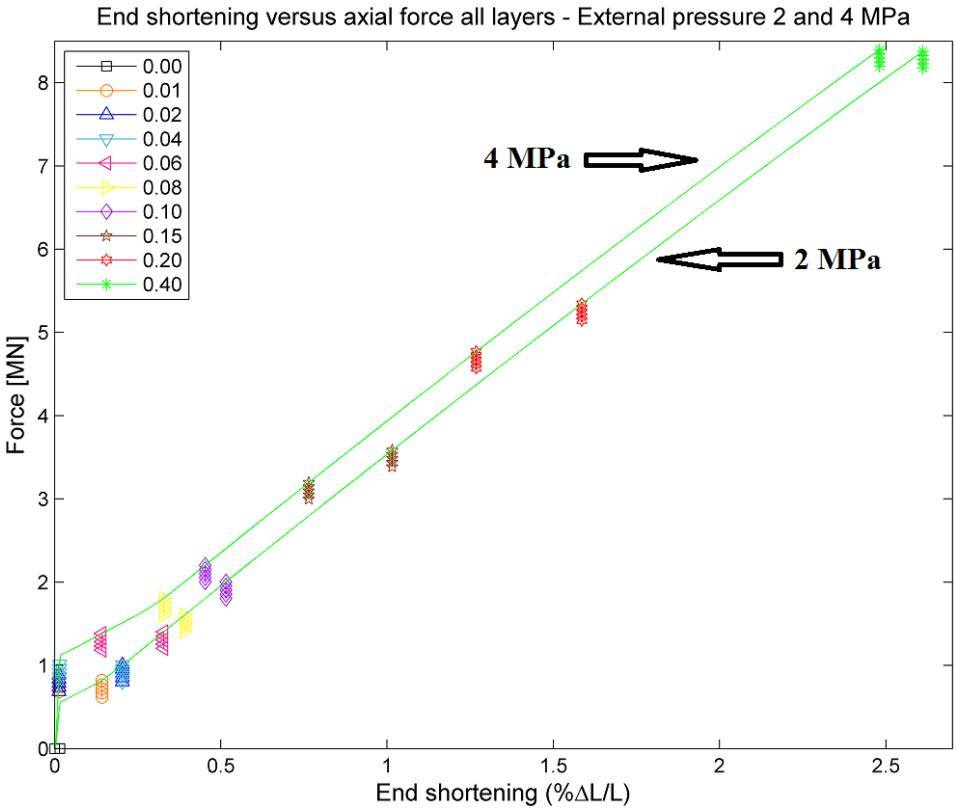

Figure 8.1: Case 1: End shortening versus axial force in all layers of the cross section

As seen in figure 8.1 the buckling force is in the range of 0 MN to 2.5 MN when the friction factor is 0.1 and lower. For increasing friction factors the buckling load is drastically increased. For the highest friction factor of 0.4 the accompanied buckling load is just above 8 MN and the corresponding end shortening is approximately 2.5%. An end shortening of 2.5% is approximately 125 mm. Another thing to notice is that the buckling load is actually lower when the external pressure is 4MPa than 2MPa for the analyses with friction factors of 0.15 and 0.2.

To identify the accompanying buckling modes the 3D-mesh of the model is used. For the case with external pressure of 4 MPa and a friction factor of 0.4 the analysis stops after 61 seconds.

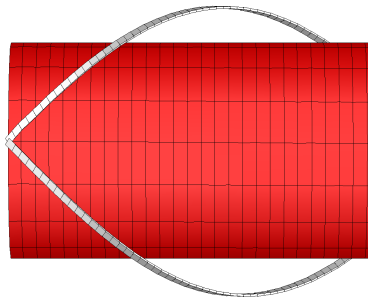

Figure 8.2: Tensile armour wires right before buckling occurs. External pressure 4 MPa and friction factor 0.4

Using a displacement scaling factor of 10 on the model in figure 8.2 right before buckling occurs we can see that the tendons have moved radially outwards. This might indicate that the accompanying buckling mode is bird-caging as described in chapter 2.4.1. The same observations were made for the case with exernal pressure 4 MPa and friction factors of 0.20.

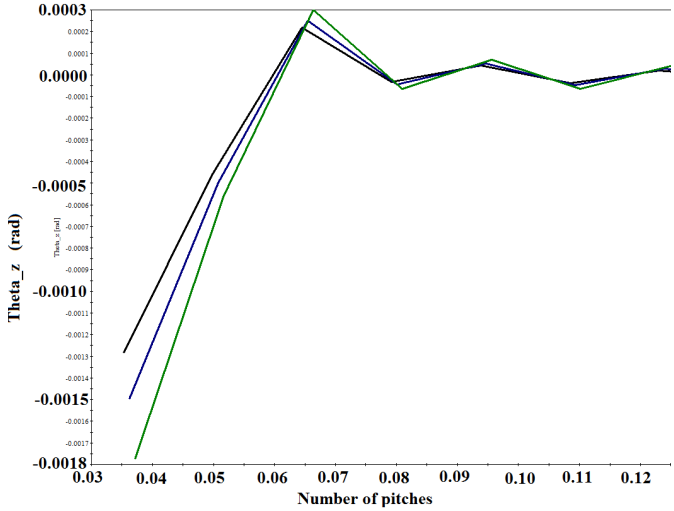

Figure 8.3: Pitch versus angle between wire and pipe axis. External pressure 4 MPa and friction factor 0.4

In figure 8.3 the angle between the wire and pipe axis is plotted versus the number of pitches for the final three timesteps before buckling. We can see that the the angle at the end of the pipe is very large compared to the rest of the pipe. This might indicate that buckling occurs at the end of the pipe first and that the buckling mode might not be radial as suggested by figure 8.2.

For the case with an external pressure of 4 MPa and friction factor of 0.15 the

analysis does not stop when buckling occurs making it possible to investigate the behaviour of the wires after buckling.

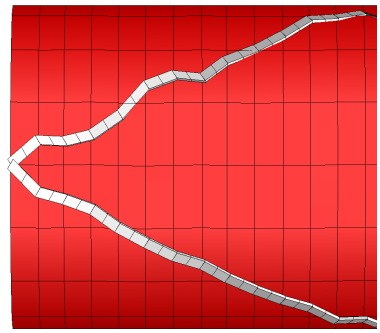

Figure 8.4: Tensile armour wires right after buckling occurs. External pressure 4 MPa and friction factor 0.15

The wires in figure 8.4 may indicate that the wire buckling is initiated at the end of the pipe. This might be a result of torsion of the pipe core since the wires are forced to follow the core. The same trend with buckling at the end of the pipe can be seen for the other cases with 4 MPa external pressure and low friction factors.

Another thing that is noticed is that the internal wire sometimes move into the pipe wall when the external pressure is applied.

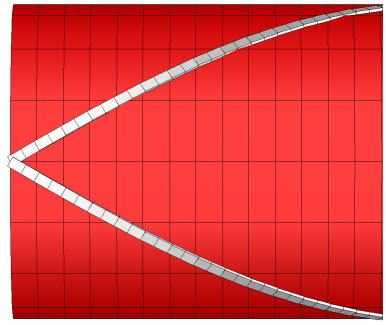

Figure 8.5: Tensile armour wires right moving into the pipe core. External pressure 4 MPa and friction factor 0.04

As can be see from both figure 8.4 and figure 8.5 the armour wires have pierced the pipe core. This may suggest that the stiffness of the pipe core should be increased.

When the external pressure is 2 MPa and the friction factor is 0.2 a buckling load of 5.54 MN is recorded.

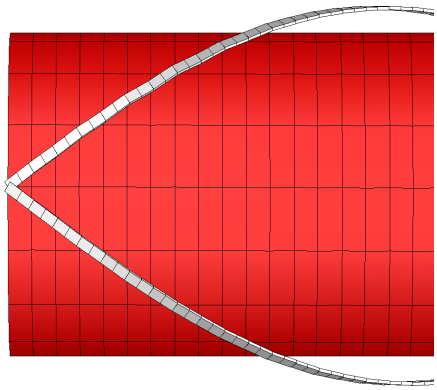

Figure 8.6: Tensile armour wires right after buckling occurs. External pressure 2 MPa and friction factor 0.20

Looking at figure 8.6 the same trend as for the case with external pressure of 4 MPa is seen. The wires are moving radially outwars, but the bucklin seems to be initiated at the end of the pipe.

Also for an external pressure of 2 MPa and low friction factors it seems like the wires move through the pipe wall as seen in figure 8.7.

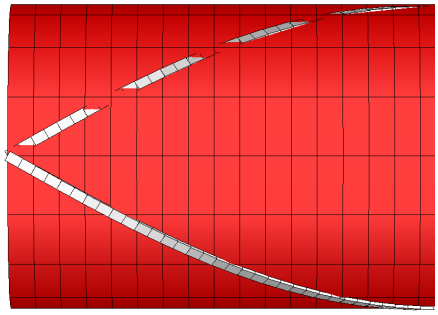

Figure 8.7: Tensile armour wires right after buckling occurs. External pressure 2 MPa and friction factor 0.04

8.2 Case 2

When the external pressure is applied as nodal loads acting on springs connected to the inner tensile armour wire the following figure of the end shortening versus axial force is obtained.

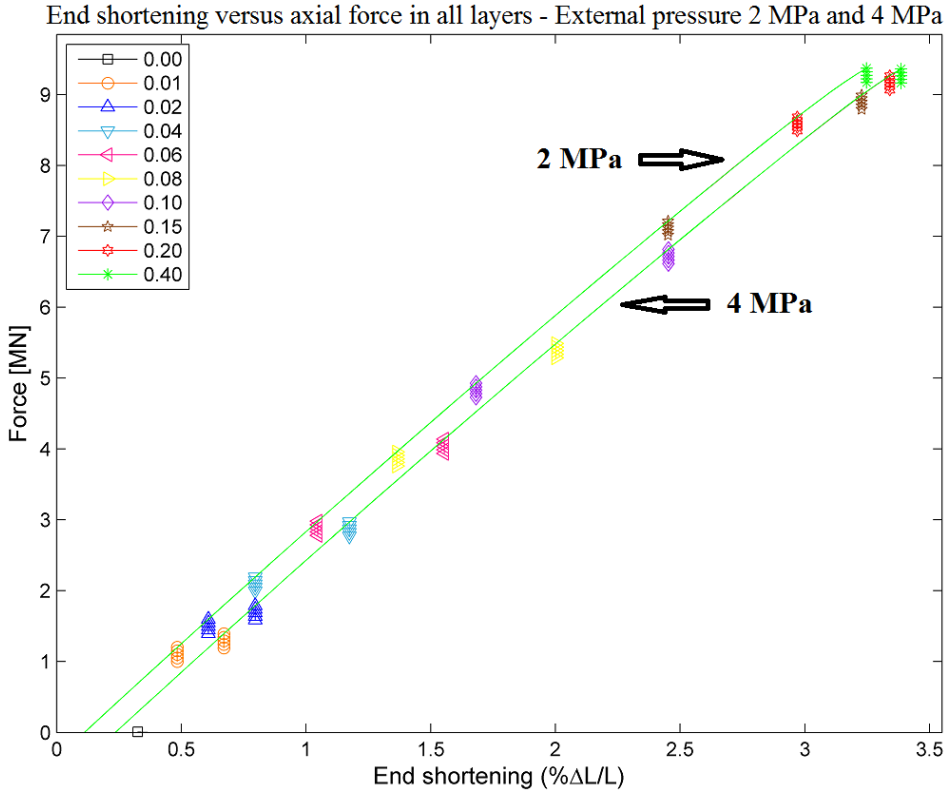

Figure 8.8: Case 2: End shortening versus axial force in all layers of the cross section

If we take a look at the slope of the curves in figure 8.8 and figure 8.1 they seem to be quite similar. The slope for the curves in figure 8.1 is approximately 3 when looking at the curve for end shortenings above 0.5%. The slope for the curves in figure 8.8 is also approximately 3.

When comparing the buckling loads in figure 8.8 with figure 8.1 it is seen that the buckling loads are higher in the case where the external pressure is applied to the inner wires. The largest relative differences are seen for the smallest friction factors, but also the highest friction factors get an increase in the buckling load. It is also noted that for the highest friction factor the end shortening is above 3

In order to determine the buckling modes of the wires the 3D-mesh is used. For the analysis using an external pressure of 4 MPa and a friction factor of 0.4 the mesh of the model right before buckling is viewed.

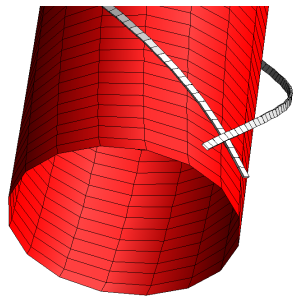

Figure 8.9: Tensile armour wires right before buckling occurs. External pressure 4 MPa and friction factor 0.4

When using a displacement scaling factor of 5 it can be seen from figure 8.9 that the pipe core has experienced a large rotation. This might suggest that the wires buckle because of torsion.

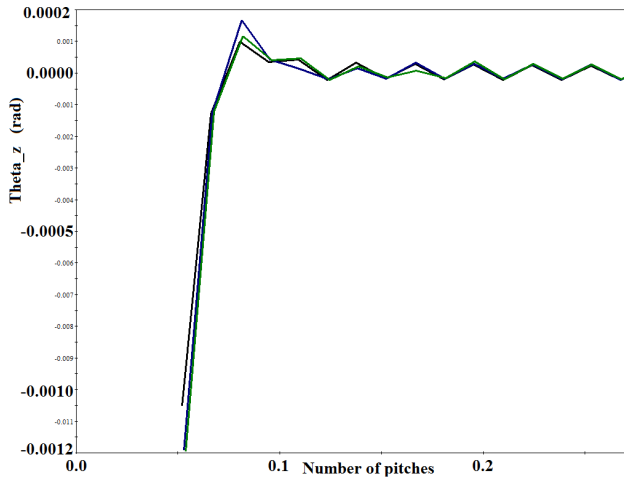

Figure 8.10: Pitch versus angle between wire and pipe axis. External pressure 4 MPa and friction factor 0.4

When looking at the θ_z angle versus the pitch length it is again seen that the angle is significantly larger on the pipe end. Again this suggests that buckling is initiated at the end of the pipe.

For low friction factors the results are similar to case 1 where the buckling of the wires seems to be initiated at the end of the pipe.

8.3 Case 3

When the external pressure is applied as a pre described displacement on the outer wires the following figure of the end shortening versus axial force inn all layers is obtained.

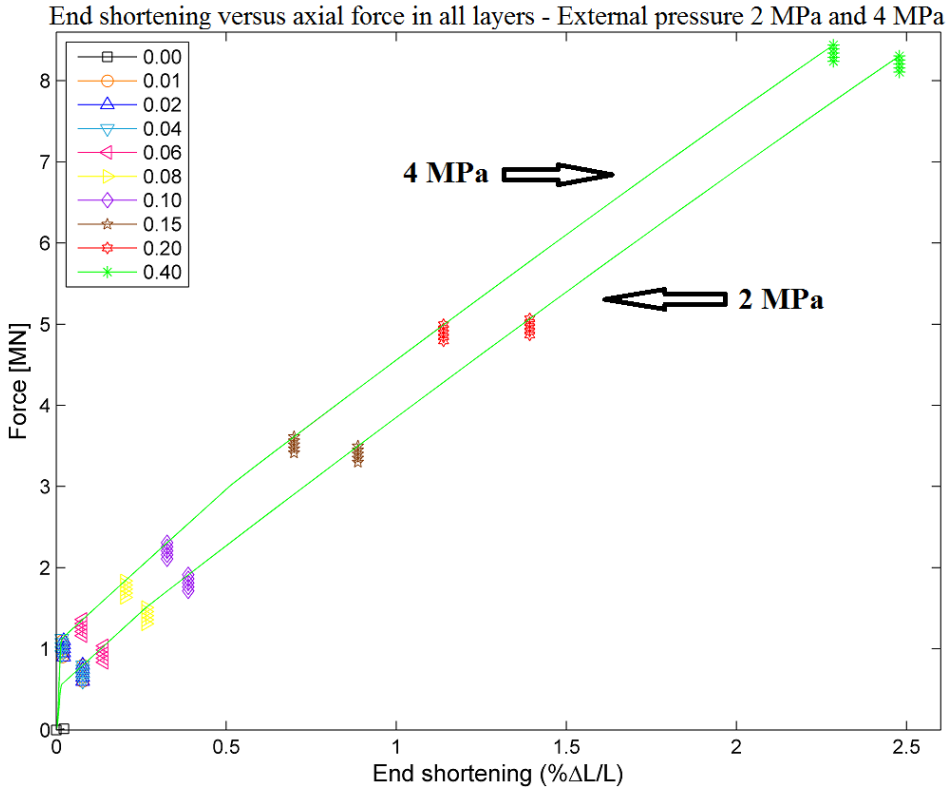

Figure 8.11: Case 3: End shortening versus force in all layers of the cross section for all friction factors

As we can see when comparing figure 8.11 with 8.1 the maximum buckling load and the end shortenings obtained for the friction factor of 0.4 is approximately the same. The inclination of the curves are also almost identical. This indicates that modelling the external pressure as nodal point forces or as nodal point displacements yields the same results.

Again we take a look at the the 3D-mesh.

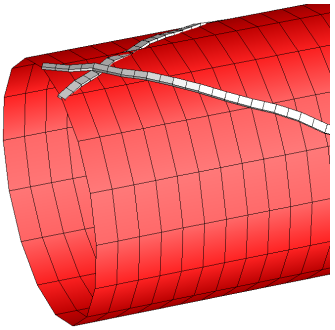

Figure 8.12: Tensile armour wires right after buckling has occurred. External pressure 4 MPa and friction factor 0.02

From figure 8.12, from the analysis using a friction factor of 0.02 and an external pressure of 4 MPa, the buckling of the wires also seem to be initiated at the end of the pipe. It can also be seen that the inner wire go through the pipe core, indicating that the stiffness used for the core may need to be adjusted. The same pattern can be seen in all the analyses for both 2 MPa and 4 MPa.

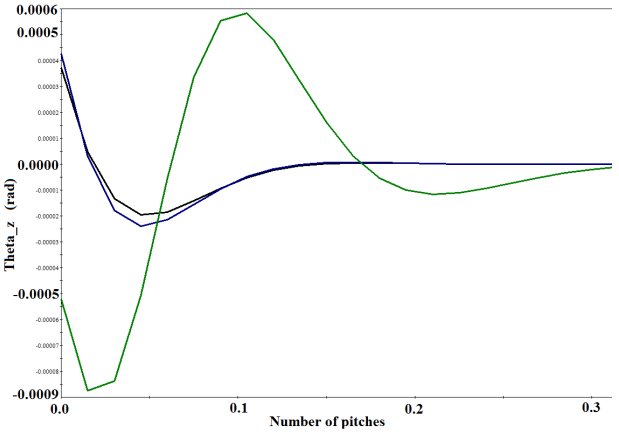

Figure 8.13: Pitch versus angle between wire and pipe axis. External pressure 4 MPa and friction factor 0.02

When looking at the pitch length versus the angle between the wire and the pipe axis θ_z for the last three time steps before buckling occurs the observation that buckling is initiated at the end of the pipe is supported.

For high friction factors the same twist of the pipe as in figure 8.9 is noticed, suggesting that buckling might be as a result of torsion.

8.4 Comparing the buckling loads for the different cases

For the three different cases studied the only difference is how the external pressure is applied. The resulting end shortening versus buckling load curves generated from the results all have an inclination of 3. The buckling loads for the different cases were however not the same.

Table 8.4: Comparing the buckling loads for the 8.1, case 8.2 and case 8.3 for external pressure of 2 MPa.

Friction factor	**Case 1**	**Case2**	**Case3**
0.00	0.01	0.01	0.04
0.01	1.00	1.40	1.03
0.02	1.20	1.80	1.03
0.04	1.20	2.39	1.03
0.06	1.60	3.17	1.27
0.08	1.80	4.15	1.72
0.10	2.20	5.12	2.11
0.15	3.78	7.40	3.7
0.20	5.54	8.85	5.26
0.40	8.56	9.40	8.49

From table 8.4 the buckling loads from external pressure of 2 MPa for the three different cases are compared. It is observed that Case 1 and Case 3 have approximately the same buckling loads. Another thing to take notice from the table is that for case 1 the buckling loads are identical for friction factors of 0.02 and 0.04. For case 3 the buckling loads are identical for friction factors of 0.01, 0.02 and 0.04. No clear understanding of the reason for this was found from studying the 3D visualisation of the model. This is something that should be investigated further.

When comparing case 1 and case 3 with the buckling loads from case two it is observed that the general trend is that case 2 yields higher buckling loads. In case 1 and case 3 the external pressure is applied on the outer wire, while for case 2 it is applied on the inner wire. The results seem to indicate that applying the external pressure on the inner wire would yield higher buckling loads. It would be expected that the resulting buckling loads from all three cases would be approximately the same, so this is something that must be investigated further.

When comparing the results from case 1, case 2 and case 3 with an external pressure of 4 MPa the same trends are observed. Case 1 and case 3 yield approximately the same buckling loads and case 2 yields a higher buckling load.

8.5 Investigating the effects of torsion

The analyses are carried out with external pressure applied as nodal loads on the outer wire in the same manner as in chapter 8.1. The difference in these analyses is that the pipe core is restrained from torsion.

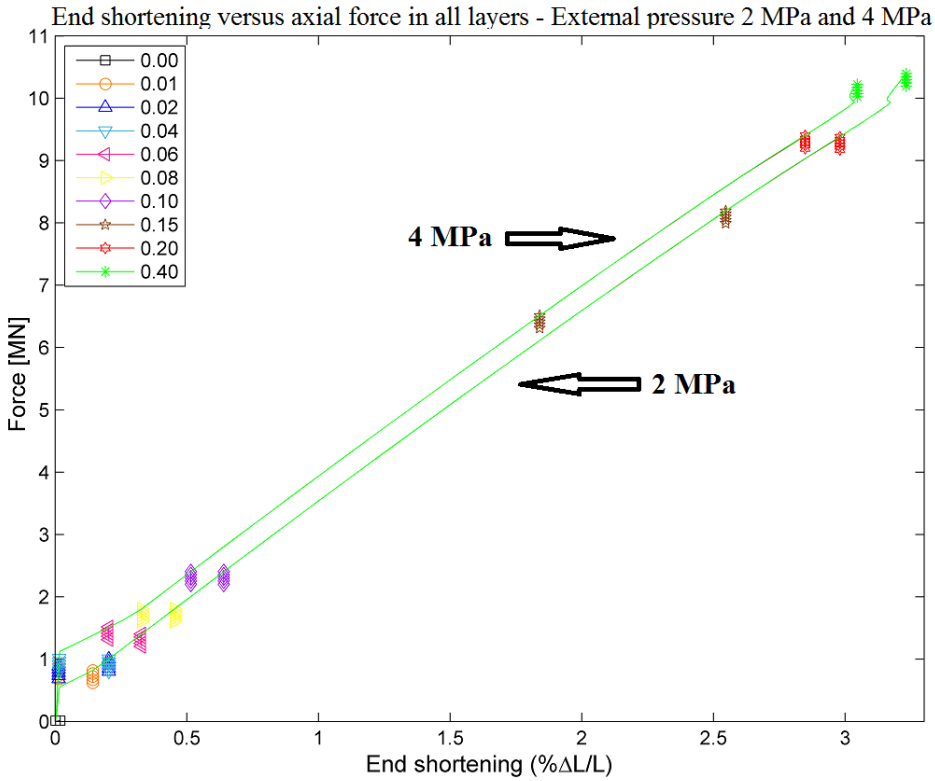

Figure 8.14: Case 4: End shortening versus force in all layers of the cross section for all friction factors

When comparing figure 8.14 with figure 8.1 from case 1 we can see that the maximum buckling loads have increased by approximately 2 MN for the highest friction factor. The friction factors of 0.2 and 0.15 has also experienced a large increase in the buckling loads. For the lowest friction factors the buckling loads have increased minimally.

Table 8.5: Comparing the buckling loads and end shortenings from case1 and case 4 for external pressure of 2 MPa.

Friction factor	**Figure 8.1**	**Figure 8.14**	**Difference (%)**
0.00	0.01	0.01	0
0.01	0.8	0.8	0
0.02	1.0	1.0	0
0.04	1.0	1.0	0
0.06	1.4	1.4	0
0.08	1.6	1.8	12.5
0.10	2.0	2.3	15
0.15	3.6	8.2	128
0.20	5.3	9.2	74
0.40	8.2	10.3	26

In table 8.5 buckling loads for case 1 and case 4 are compared for an external pressure of 2 MPa. It is clearly seen that for the five lowest friction factors the buckling loads are not influenced by restraining the pipe from torsion. This suggests that buckling experienced in case 1 for the lowest friction factors was not result of torsion.

For the highest friction factors the buckling loads are increased, some of them dramatically. This indicates that torsion has had a clear influence on the buckling loads for the analyses in case 1 using a high friction factor.

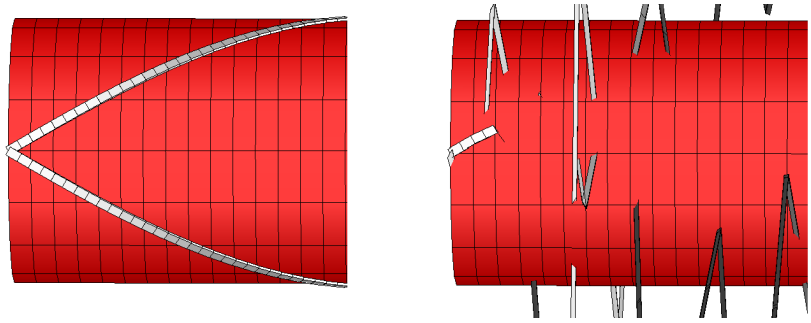

Figure 8.15: Wire before and after buckling. External pressure 2 MPa and friction factor 0.04

In figure 8.15 end of the pipe cross section is seen right before and right after buckling. An external pressure of 2 MPa and friction factor of 0.04 is used. From this figure it is difficult to determine the buckling mode.

The friction factor of 0.15 is the case where the increase between the analysis with and without torsion is largest.

Using a displacement factor of 5 at the middle of the model it might seem like

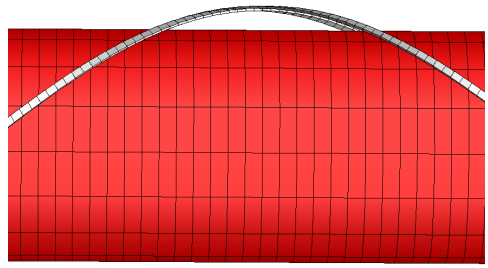

Figure 8.16: Model right before buckling. External pressure 2 MPa and friction factor 0.15

the accompanied buckling load is bird-caging. The same observations are made for friction factors of 0.2 and 0.4.

Table 8.6: Comparing the buckling loads and end shortenings from figure 8.1 and figure 8.14 for external pressure of 4 MPa.

Friction factor	**Figure 8.1**	**Figure 8.14**	**Difference (%)**
0.00	0.01	0.01	0
0.01	0.8	0.8	0
0.02	0.8	0.8	0
0.04	1.0	1.0	0
0.06	1.3	1.5	15
0.08	1.8	1.8	0
0.10	2.2	2.4	9
0.15	3.2	6.3	97
0.20	4.9	9.1	86
0.40	8.2	10.2	24

In table 8.6 buckling loads for 4 MPa external pressure from figure 8.1 and figure 8.14 are compared. The same trend is seen as for the comparison of the cases using 2 MPa. For the lowest friction factors there is no difference, and for the highest friction factors the differences are significant.

Another observation from table 8.6 is that there is an increase in the buckling loads for the friction factor of 0.06, but not for the friction factors 0.04 and 0.08.

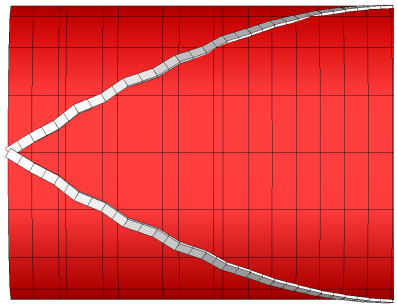

Figure 8.17: Model right before buckling. External pressure 4 MPa and friction factor 0.06

In figure 8.17 a displacement scaling factor of 15 is applied to the model with friction factor 0.06 which is exposed to external pressure of 4 MPa . Looking at the end of the pipe it looks like the initiation of buckling starts with a "wrinkling" of the wires.

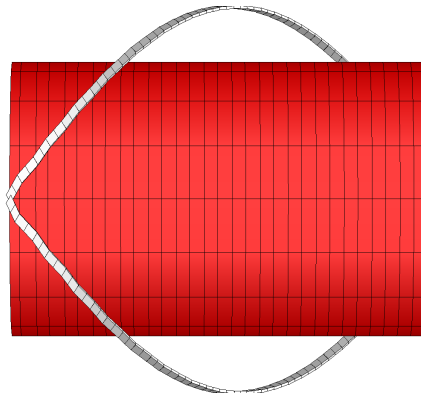

Figure 8.18: Model right before buckling. External pressure 4 MPa and friction factor 0.4

In figure 8.18 a displacement factor of 10 is used on the model with friction factor 0.4 and external pressure 4 MPa. Again it is seen that the wires have moved radially outwards, but taking a closer look at the end of the pipe it is noticed that the "wrinkling" phenomenon is apparent also here.

When restraining the models used in chapter 8.2 and chapter 8.3 from torsion the same observations are made as when comparing the model in chapter 8.1 with torsion with the one in chapter 8.5 without. It is observed that for the lowest friction factors the applied forces lead to the "wrinkling" phenomena in the wires at the end of the pipe causing them to buckle. When the friction factors are increased the wires start to move radially outwards, indicating that a bird-caging buckling mode may be building up, but the "wrinkling" phenomena is present in

the wires at the ends of the pipe also here.

The reason for the "wrinkling" is something that should be investigated further. One possible explanation of the phenomena is the boundary conditions used. One approach to determine if this is the base is to vary them systematically. The phenomena may also be due to some effects when the different layers in the model interact. This should also be investigated further.

8.6 Buckling loads for higher external pressures

Analyses were carried out using the model from Case 1 but this time letting the external pressures range from 2 MPa to 15 MPa. A constant friction factor of 0.4 was used.

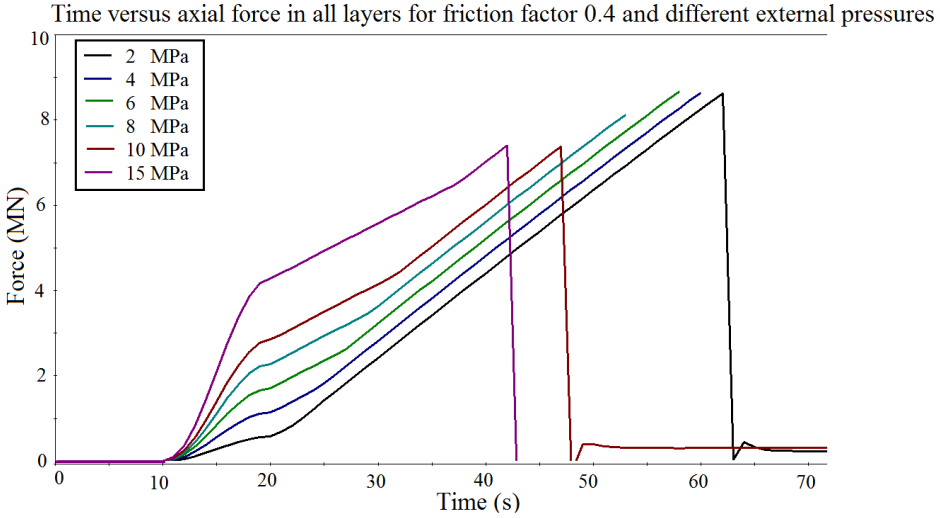

Figure 8.19: Tensile armour wires right moving into the pipe core

As seen from figure 8.19 the maximal buckling load seems to decrease as the external pressure is increased beyond 6 MPa. This is opposite of what would be expected and does not seem plausible. Looking at the curves it seems like the model used is capable of capturing the effects of the external pressure in a correct manner, but when the end compression is applied this does not seem to be the case. This is something that should be investigated further by a more extensive study on how the model reacts.

Analyses were also carried out using the model from Case 2 and letting the external pressures range from 2 MPa to 15 MPa. A constant friction factor of 0.4 was again used.

As seen from figure 8.20 the maximum values for the different external pressures are approximately the same for the different external pressures. It can also be seen that when the external pressure is applied a pressure force is experienced in the wires. This might be the reason why higher buckling loads are experienced in case 2 compared to case 1 and case 3.

In case 2 the external pressure is applied on the inner wires. By doing this the method described in chapter 6.8 might not generate graphs that are directly comparable to the graphs by Vaz and Rizzo [7] as can be seen in figure 3.2. One possibility to generate a similar graph may be to apply the external pressure using a static analysis between 10 and 20 seconds and then restarting the analysis with a stress free cross section. This might lead to more comparable results according to figure 3.2.

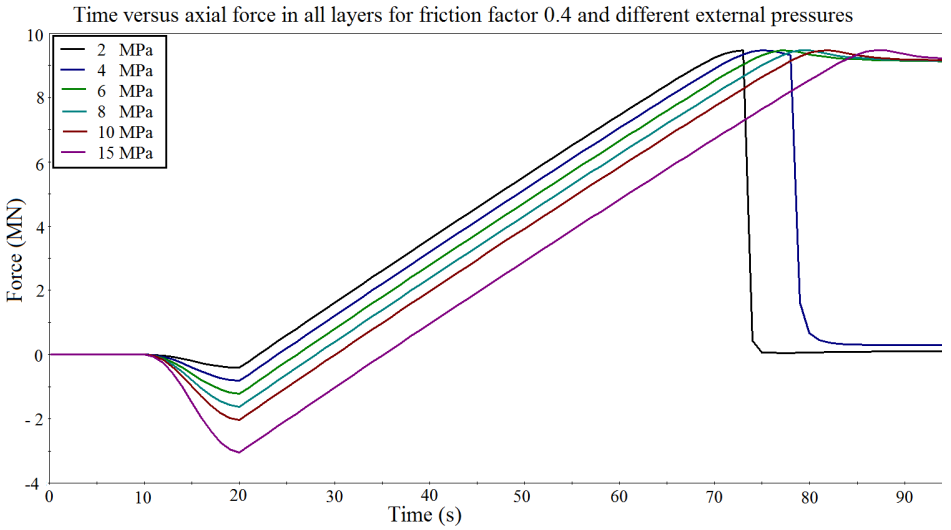

Figure 8.20: Tensile armour wires right moving into the pipe core

The same analysis with external pressures ranging from 2 MPa to 15 MPa and a friction factor of 0.4 were performed on case 3 and case 4. The results from the analyses can be seen in figure 8.22 and 8.21. Again it is observed that increasing the pressure does not lead to higher buckling loads as would be expected. This should be further investigated.

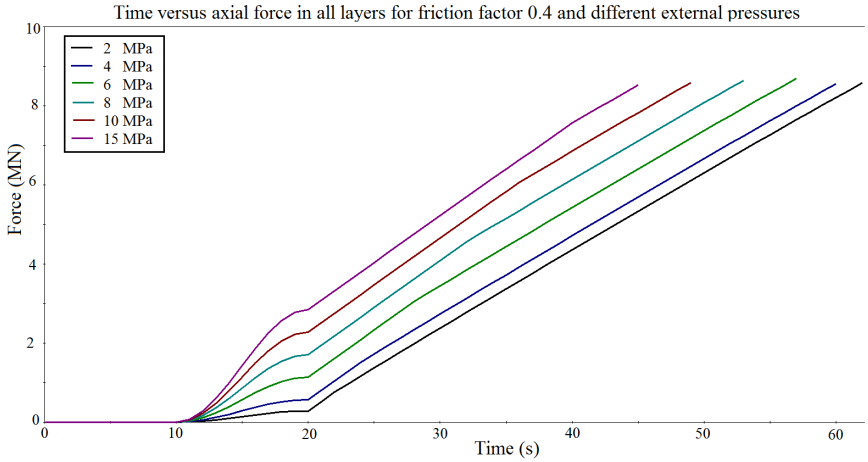

Figure 8.21: Tensile armour wires right moving into the pipe core

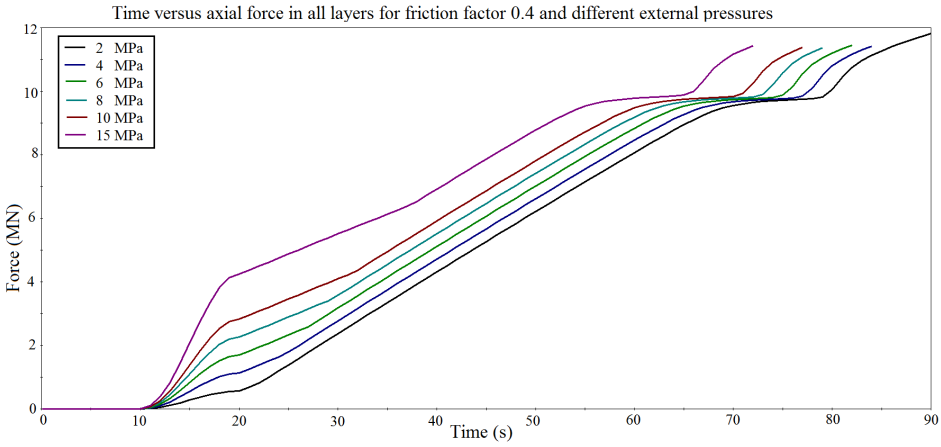

Figure 8.22: Tensile armour wires right moving into the pipe core

8.7 Comparing with the results by Vaz and Rizzo

If we take a look at the graphs obtained in figure 8.1, figure 8.8 and figure 8.11 it is seen that the inclination of the curves are approximately three for all of them. The differences between them is mainly where they start.

When comparing to the curves obtained by Vaz and Rizzo [7] the curves from figure 8.1 are chosen. When comparing them the time of buckling is not considered, only the inclination of the curves.

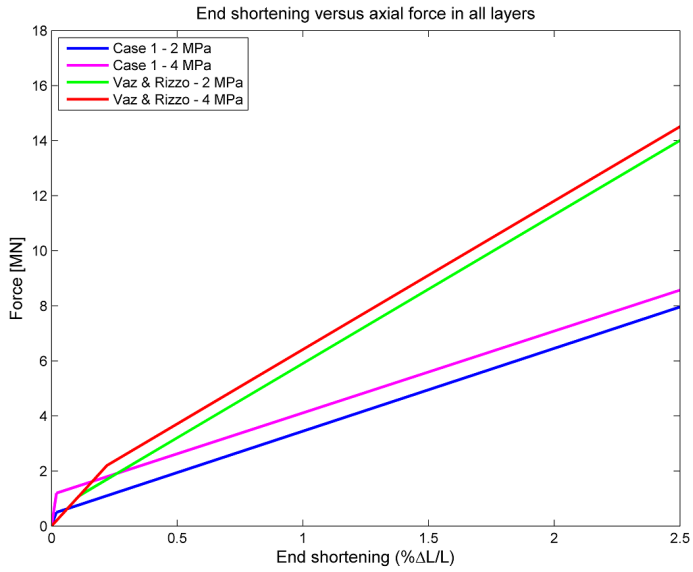

Figure 8.23: Comparing curves in figure 8.1 with curves by Vaz and Rizzo [7].

In figure 8.23 the curves by Vaz and Rizzo are extrapolated up to the point where the end shortening is 2.5% in order to compare them to the curves in figure 8.1. It is seen that the inclination of the curves by Vaz and Rizzo are approximately 5.3 and the inclination of the curves from figure 8.1 is 3.

In the article by Vaz and Rizzo the formula used to calculate the axial compressive force is [7]:

$$F_z = \frac{f_{z,i}}{\cos^2(\alpha_i)} + \frac{f_{z,e}}{\cos^2(\alpha_e)} \tag{8.1}$$

In the formula $f_{z,i}$ and $f_{z,e}$ are the reaction forces in the inner and outer wires and α_i) and α_e) are the lay angles of the inner and outer wire.

Vaz and Rizzo uses z-coordinates along the pipe axis whereas in this thesis the x-coordinates are along the pipe axis. In this thesis the axial compressive force is given by the following equation:

$$F_{x,original} = f_z \cos\alpha \tag{8.2}$$

In order to compare the axial compressive forces from this thesis to the ones in the article by Vaz and Rizzo the following adjustment can be made:

$$F_{x,compared} = \frac{F_{x,original}}{\cos^3\alpha} \tag{8.3}$$

Since the lay angle α is 30° dividing the original results by this factors equals multiplying the results by approximately 1.54.

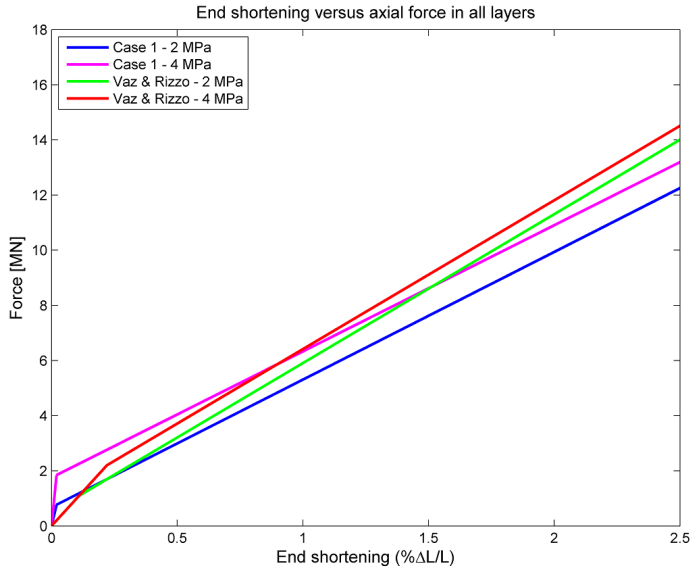

Figure 8.24: Comparing curves in figure 8.1 with curves by Vaz and Rizzo [7] with consideration of lay angle.

The new curve of the results in this thesis now has an inclination of 4.6 as seen in figure 8.24. This suggests that the stiffness used in the models created in this thesis is slightly smaller than the stiffness used by Vaz and Rizzo. By modifying the stiffness it should be possible to generate the exact same inclination of the curves.

8.8 Varying the slip distance

As seen in the graphs created the buckling loads obtained in chapter 8.1, chapter 8.2,chapter 8.3 and chapter 8.5 are very high compared to the values obtained by Vaz and Rizzo [7]. Many factors can affect when the buckling occurs. One of the most important factors for this is the slip distance before friction is enabled. No details about this value is given in about the model used in the article by Vaz and Rizzo [7].

In the model used for the analyses in the slip distance used has been 0.1 mm. In order to demonstrate the effect of this value som analyses are carried out with different slip distances for the case using an external pressure of 4 MPa and a friction factor of 0.4.

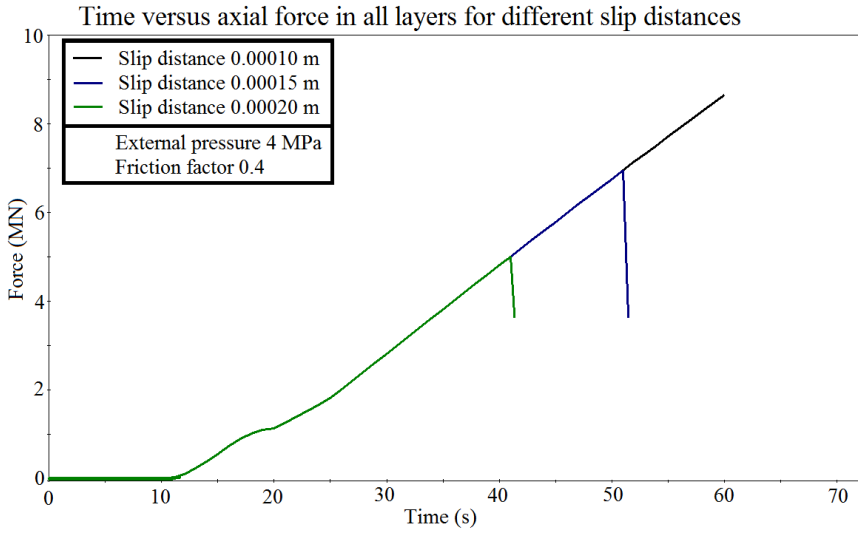

Figure 8.25: Systematically varying the slip distance to see when buckling occurs.

As seen in figure 8.25 the maximum buckling load drops by 2 MN when increasing the slip distance by 50%. If the slip distance is doubled the drop in maximum buckling load is almost 4 MN. From this it is clear that the slip distance is a key parameter when performing parametrical studies varying the friction factor and the external pressure.

By tuning the slip distance and the stiffness of the springs used it should be possible to recreate the exact same results as in the article by Vaz and Rizzo [7]. This clearly illustrates the importance of stating all assumptions and input parameters when describing models used for analysis.

9 Conclusions

When creating FEM-models used to study the behaviour of flexible pipe cross section it is important to state all the assumptions and input parameters used. Doing this makes recreating the model possible without having to assume key parameters. In the article by Vaz and Rizzo [7] not all the information needed to recreate the model is given. The model created in this thesis is assumed to be similar to the one created in the article by Vaz and Rizzo, but this might not be the case since important input parameters may be different. This makes it difficult to compare the results obtained using the different models.

When doing buckling analyses on flexible pipe armouring wires it is important to define key aspects of the model and input parameters in a correct manner. A way of doing this is to perform sensitivity studies in an early phase when creating the model. One of the key parameters to be aware of when studying the buckling capacity of the wires is the element length. The element length should be chosen to avoid avoid local buckling of the wires. Setting the element length to high can lead to the results obtained not being valid.

When applying the the external pressure to the model three different approaches were tested. In the first case the external pressure was applied directly to the outer wires by applying a nodal point force to springs connected to the wire. In the second case the external pressure is applied in the same way, but this time the springs are connected to the inner wire. The third approach applied the external pressure as a pre described displacement directly on the outer wire. The results from the first and third approach were almost exactly the same, while the result from the second approach yielded a similar inclination of the curve but slightly larger buckling loads.

When looking at the 3D models of the results could seem like buckling occurred as a result of torsion. To study this new analyses were carried out using the same models but restraining the pipe from torsion. When restrained from torsion the inclination of the curves remained the same, but the accompanied buckling loads were slightly larger for the highest friction factors. From this it may be assumed that the reason for buckling was torsion for the highest friction factors in the three first cases.

How the pre described displacements are imposed on the wire ends seem to have a very large effect on the result. When applying pre described displacements directly to the pipe core it seems that the buckling of the wires is initiated at the end of the pipe. This can be seen from both the 3D visualisation of the model and from the graphs of the number of pitches versus the angle between the wire and the pipe axis, θ_z.

For low friction factors and high external pressures and the wires buckle while applying the external pressure. The actual buckling mode is difficult to obtain, but again it seems like the buckling is initiated at the end of the pipe. In addition it is seen that the wires moves into the pipe wall. This might indicate that the stiffness between the pipe wall and the inner armour wires is too low.

When comparing the buckling loads and accompanied end shortenings obtained in this thesis with the results obtained by Vaz and Rizzo [7] it is seen that values

obtained in this thesis are higher for both buckling loads and end shortenings. If we however only consider the inclination of the curves it is seen that the inclination of the curves in by Vaz and Rizzo is 5.3 as opposed to 3 for the curves generated in this thesis. This indicates that the values used for the springs in the two models might be different. If the spring stiffness is modified it should be possible to obtain the exact same inclination as in the curves by Vaz and Rizzo.

By varying the slip distance it was observed that increasing the slip distance resulted in significantly lower buckling loads. Doubling the slip distance led to a reduction in the buckling load of approximately 40%. In the article by Vaz and Rizzo [7] the slip distance used has not been given. This suggests that tuning the slip distance and the spring stiffness it should be possible to obtain the exact same results. This clearly illustrates the importance of being detailed when describing the models and assumptions being used when carrying out analyses.

9.1 Recommendations for further work

When performing sensitivity analyses on the number of elements it was indicated that the buckling loads when using 200 and 400 elements were the same. The number of cases studied for this might be to low to be certain that 200 elements is enough. A full study of the cases should be performed using both 200 and 400 elements to see if all the results will be the same. It might also be interesting to increase the number of elements even more than 400.

A possibility that could be tested for the external pressure is to apply it by using a static analysis for the first 20 seconds instead of a dynamic analysis, and then restarting the analysis when applying the end compression.

How the pre described displacements are imposed to the wire ends seem to have a very large effect on the results. When applying pre described displacements directly to the pipe core it seems that the buckling of the wires are initiated at the end. By applying the end compression directly on the wires it could be investigated if this yields different results.

For large external pressures it is noticed that the wires buckle before the end compression is applied. The wires seem to move into the pipe wall. The stiffness used for the pipe wall could be increased systematically to see if the results are affected.

When applying external pressures beyond 4 MPa it would be expected that the maximum buckling loads would increase. Instead the maximum buckling loads are the same for both 2 MPa and 4 MPa external pressures, and in some cases even lower for 15 MPa than 2 MPa. This does not seem plausible and should be investigated further.

References

[1] A. Coutarel F. Becarte. Instability of tensile armour layers of flexible pipes under external pressure. In *Proceedings of OMAE2004, 23rd International Conference on Offshore Mechanics and Arctic Engineering.*

[2] P. Secher F. Bectarte and A. Felix-Henry. Lateral buckling of armor wires in flexible pipes: Reaching 3000m water depth. In *Proceedings of OMAE2011, 30th International Conference on Offshore Mechanics and Arctic Engineering.*

[3] P. Secher F. Bectarte and A. Felix-Henry. Qualification testing of flexible pipes for 3000m water depth. In *Offshore Technology Conference 2011.*

[4] American Petroleum Institute. *Recommended Practice For Flexible Pipe.* ANSI/API Recommended Practice 17B, fourth edition, June 2008.

[5] ISO. *Petroleum and natural gas industries - Design and operation of subsea production systems - Part 2: Unbonded flexible pipe systems for subsea and marine applications.* International organization for standarisation, second edition, July 2006.

[6] G.B Ellwanger J.R.M de Sousa, A.N Pinho and E.C.O Lima. Numerical analysis of a flexible pipe with damaged tensile armor wires. In *Proceedings of OMAE2009, 28th International Conference on Offshore Mechanics and Arctic Engineering.*

[7] N.A.S. Rizzo M.A. Vaz. A finite element model for flexible pipe armour wire instability. In *Marine Structures 24 (2011) p 275-291.*

[8] P. Kalaeff M.P. Braga. Flexible pipe sensitivity to birdcaging and armour wire lateral buckling. In *Proceedings of OMAE2004, 23rd International Conference on Offshore Mechanics and Arctic Engineering.*

[9] J.H. Andreasen N.H. Østergaard, A. Lyckeggaard. On lateral buckling failure of armour wires in flexible pipes. In *Proceedings of the ASME 2011 30th International Conference on Ocean, Offshore and Arctic Engineering, OMAE2011.*

[10] Nils Rune Sødahl. *Methods For Design And Analysis Of Flexible Risers.* PhD thesis, Norges Tekniske Hoegskole, 1992.

[11] S. Sævik and M.J. Thorsen. Techniques for predicting tensile armour buckling and farigue in deep water flexible risers. In *To be puclished in Proceedings of OMAE2012, 31st International Conference on Offshore Mechanics and Arctic Engineering.*

[12] Svein Sævik. *On Stresses And Fatigue In Flexible Pipes.* PhD thesis, Norges Tekniske Hoegskole, 1992.

[13] Svein Sævik. *BFLEX 2010 - Theory manual.* Sintef - Marintek, 2010.

[14] T.G Syvertsen and P.G Bergan. *Knekning av søyler og rammer*. Tapir Forlag, 1978.

[15] C. Loper Z. Tan, T. Sheldrake and G. Karabelas. Behaviour of tensile wires in unbondened flexible pipe under compression and design optimalization for prevention. In *Proceedings of OMAE2006, 25th International Conference on Offshore Mechanics and Arctic Engineering*.

A Matlabscript: inputwriter.m

The Matlabscript generating the go-analyze file in Appendix B

```
vazvariasjon = 2;
beskrivelse = 'gange_';
inputfric = 0.1;
inputpex = 2;
stivhetsred = 1;
pdispfac = 1;

if vazvariasjon == 0
    analyser = 8;
elseif vazvariasjon == 1
    analyser = 20;
elseif vazvariasjon == 2
    analyser = 1;
else
    analyser = 10;
end

inputfilnavn = 'vazv2_';
friksjonsvektor = [0 0.01 0.02 0.04 0.06 0.08 0.1 0.15 0.2 0.4];
pekstvektor = [2 4];
pekstvektoralle = [0 1 2 4 6 8 10 15];
multianalysenr = 1;

ut = fopen('go-analyze', 'w');
tekst = '#! /bin/sh';
fprintf(ut,'%s \n \n' , tekst);

T = clock; aar = T(1); mnd = T(2); dag = T(3); timen = T(4); minutt =
    T(5);

fprintf(ut,'mkdir Analyse\n');
fprintf(ut,'cp go-analyze Analyse/go-analyze\n',inputfilnavn);
fprintf(ut,'cp go-plot Analyse/go-plot\n');
fprintf(ut,'cp %s%i.2bif Analyse/%s%i.2bif\n',inputfilnavn,
    multianalysenr, inputfilnavn, multianalysenr);
fprintf(ut,'cp mplot_oc.2bpi Analyse/mplot_oc.2bpi\n');
fprintf(ut,'chmod -R a+r,u+w Analyse\n');
fprintf(ut,'cd Analyse\n');
fprintf(ut,'mkdir matrixplots\n\n');

nant = analyser; teller = 1; tall = 1;

for nr = 1:analyser

if nant == 1
    friksjon = inputfric;
    pekst = inputpex;
else
    if vazvariasjon == 1 || vazvariasjon == 3
    nhalf = analyser/2;
    if nr == 11 || nr == 21 || nr == 31 || nr == 41 || nr == 51 || nr
        == 61 || nr == 71
        teller = teller - 10;
```

```
51          tall = tall + 1;
52      end
53      friksjon = friksjonsvektor(teller)
54      pekst = pekstvektor(tall)
55      teller = teller + 1;
56      else
57      friksjon = inputfric
58      pekst = pekstvektoralle(nr)
59      end
60  end
61
62  fprintf(ut,'# Analyse nr %i\n', nr);
63  fprintf(ut,'mkdir analyse%i\n', nr);
64  fprintf(ut,'cp %s%i.2bif analyse%i/input.2bif\n',inputfilnavn,
        multianalysenr, nr);
65  fprintf(ut,'cp mplot_oc.2bpi analyse%i/mplot_oc.2bpi\n',nr);
66  fprintf(ut,'cp go-plot analyse%i/go-plot\n',nr);
67  fprintf(ut,'erzatz   "#toppteksten"        "BFLEX2010 %s%i 9.5 inch
        flexible pipe case study - fric %i , pext %i"          analyse%i/
        input.2bif\n', inputfilnavn, multianalysenr, friksjon, pekst, nr);
68  fprintf(ut,'erzatz   "#fric"        "%i"          analyse%i/input.2bif\n
        ', friksjon, nr);
69  fprintf(ut,'erzatz   "#pext"        "%i"          analyse%i/input.2bif\n
        ', pekst, nr);
70  fprintf(ut,'erzatz   "#pdispfac"        "%i"          analyse%i/input.2
        bif\n', pdispfac, nr);
71  fprintf(ut,'erzatz   "#stiffred"        "%i"          analyse%i/input.2
        bif\n', stivhetsred, nr);
72  fprintf(ut,'cd analyse%i\n',nr);
73  fprintf(ut,'bflex2010 << eod\n');
74  fprintf(ut,'input\n');
75  fprintf(ut,'eod\n');
76  fprintf(ut,'. go-plot\n');
77  fprintf(ut,'cd ..\n');
78  fprintf(ut,'mkdir matrixplots/analyse%i\n', nr);
79  fprintf(ut,'cp -R analyse%i/matrixplots_original matrixplots/analyse%i
        \n', nr, nr);
80  fprintf(ut,'mv analyse%i Analyse%i_fric=%i_pekst=%i\n', nr, nr,
        friksjon, pekst);
81  fprintf(ut,'\n');
82  end
83  fprintf(ut,'cd ..\n');
84  fprintf(ut,'mv Analyse Analyse_%i_%i_%i_%i_%i_%s%i\n', aar, mnd, dag,
        timen, minutt, beskrivelse, multianalysenr);
85  fclose(ut);
```

B Cygwin scripts: go-analyze and go-plot

Example of the start of a script that can be run in Cygwin executing multiple analysis. In line 26 the script go-plot is executed. This script can be seen on the next page.

```
1  #! /bin/sh
2
3  mkdir Analyse
4  cp go-analyze Analyse/go-analyze
5  cp go-plot Analyse/go-plot
6  cp vazv2_1.2bif Analyse/vazv2_1.2bif
7  cp mplot_oc.2bpi Analyse/mplot_oc.2bpi
8  chmod -R a+r,u+w Analyse
9  cd Analyse
10 mkdir matrixplots
11
12 # Analyse nr 1
13 mkdir analyse1
14 cp vazv2_1.2bif analyse1/input.2bif
15 cp mplot_oc.2bpi analyse1/mplot_oc.2bpi
16 cp go-plot analyse1/go-plot
17 erzatz   "#toppteksten"        "BFLEX2010 vazv2_1 9.5 inch flexible
       pipe case study - fric 1.500000e-01 , pext 2"        analyse1/
       input.2bif
18 erzatz   "#fric"        "1.500000e-01"        analyse1/input.2bif
19 erzatz   "#pext"        "2"        analyse1/input.2bif
20 erzatz   "#pdispfac"        "1"        analyse1/input.2bif
21 erzatz   "#stiffred"        "1"        analyse1/input.2bif
22 cd analyse1
23 bflex2010 << eod
24 input
25 eod
26 . go-plot
27 cd ..
28 mkdir matrixplots/analyse1
29 cp -R analyse1/matrixplots_original matrixplots/analyse1
30 mv analyse1 Analyse1_fric=1.500000e-01_pekst=2
31
32 # Analyse nr 2
33 mkdir analyse2
34 cp vazv2_1.2bif analyse2/input.2bif
35 cp mplot_oc.2bpi analyse2/mplot_oc.2bpi
36 cp go-plot analyse2/go-plot
37 erzatz   "#toppteksten"        "BFLEX2010 vazv2_1 9.5 inch flexible
       pipe case study - fric 1.500000e-01 , pext 4"        analyse2/
       input.2bif
38 erzatz   "#fric"        "1.500000e-01"        analyse2/input.2bif
39 erzatz   "#pext"        "4"        analyse2/input.2bif
```

The go-plot script used to run the BFLEX2010post analysis and move the resulting files to a seperate folder named "matrixplots_original".

```
#! /bin/sh

bflex2010post << eod
mplot_oc
eod
mkdir matrixplots_original
cp mplot_oc.2bpi matrixplots_original/mplot_oc.2bpi
mv mplot_oc-nodispx.mpf matrixplots_original
mv mplot_oc-axfor-core.mpf matrixplots_original
mv mplot_oc-condisy-12.mpf matrixplots_original
mv mplot_oc-condisy-c1.mpf matrixplots_original
mv mplot_oc-confory-12.mpf matrixplots_original
mv mplot_oc-confory-c1.mpf matrixplots_original
mv mplot_oc-epsxx.mpf matrixplots_original
mv mplot_oc-forcx-core.mpf matrixplots_original
mv mplot_oc-forcx-lay1.mpf matrixplots_original
mv mplot_oc-forcx-lay2.mpf matrixplots_original
mv mplot_oc-forcy-lay1.mpf matrixplots_original
mv mplot_oc-forcy-lay2.mpf matrixplots_original
mv mplot_oc-mz-lay1.mpf matrixplots_original
mv mplot_oc-mz-lay2.mpf matrixplots_original
mv mplot_oc-norotz-inner.mpf matrixplots_original
mv mplot_oc-norotz-outer.mpf matrixplots_original
mv mplot_oc_cz_spring.mpf matrixplots_original
mv mplot_oc-epsxx-lay1.mpf matrixplots_original
```

C Bflex2010 inputfile: vazv2_1.2bif

The script used for the analyses.

```
#
HEAD #topptekst
#-----------------------------------------------
# Control paramters
#          maxit   ndim   isolvr   npoint  ipri   conr     gacc     iproc
CONTROL     100    3      2        16      11     1.e-5    0.0      stressfree
# Control parameters for dynamic analysis
#            mstat    alpha1   alpha2   alpha
DYNCONT      2        0.0      0.09     -0.05
#-----------------------------------------------
# Nocoor input - Nodal coordinates
Nocoor Coordinates
#           no          x          y       z
              1        0.0        0.0     0.0
            201        4.9837     0.0     0.0
# Supporting first layer
Nocoor Polar
#    x0     y0    z0    b1    b2    b3    R
     0.0    0.0   0.0   0.0   0.0   0.0   0.2993/2
#    node     xcor      theta
     10001  0.00    3.1416
     10201  4.9837   -16.0984
# Outer coating
Nocoor Polar
#    x0     y0    z0    b1    b2    b3    R
     0.0    0.0   0.0   0.0   0.0   0.0   0.3053/2
#    node     xcor      theta
     20001  0.00    3.1416
     20201  4.9837   21.9912
# Springs
Nocoor Polar
#    x0     y0    z0    b1    b2    b3    R
     0.0    0.0   0.0   0.0   0.0   0.0   0.3053/2
#    node     xcor      theta
     80001  0.00    3.1416
     80201  4.9837   21.9912
# 1st structural layer
Nocoor Polar
#    x0     y0    z0    b1    b2    b3    R
     0.0    0.0   0.0   0.0   0.0   0.0   0.2993/2
#    node     xcor      theta
     30001  0.00     3.1416
     30201  4.9837   -16.0984
# 2nd structural layer
Nocoor Polar
#    x0     y0    z0    b1    b2    b3    R
     0.0    0.0   0.0   0.0   0.0   0.0   0.3053/2
#    node     xcor      theta
     40001  0.00    3.1416
     40201  4.9837   21.9912
#
Visres Integration 1 sigma-xx Sigma-xx-ax Sigma-xx-my Sigma-xx-mz
     Vconfor-z
```

```
53 #-------------------------------------------------
54 # Elcon  input
55 #-------------------------------------------------
56 # The core
57 #      group        elty        material   elementnr   node1   node2   node3
       node4
58 Elcon   core         pipe31      plastic       1          1       2
59 #       number of times   elementincrease   nodeinrease
60 Repeat          200              1                1
61 #
62 Elcon   coreh         pipe31      plastich   501    1       2
63 #       n    elinc   nodinc
64 Repeat 200    1         1
65 # Tensile Layer 1
66 #
67 # Tensile Layer 1
68 #       group          elty    flexcrossname      no    n1     n2      n3
          n4
69 Elcon   tenslayer1 hshear353    tendon     30001    1       2     30001
      30002
70                                                      repeat 200 1 1
71 # Tensile Layer 2
72 #       group          elty    flexcrossname      no    n1     n2      n3
          n4
73 Elcon   tenslayer2   hshear353    tendon     40001    1       2     40001
      40002
74                                                      repeat 200 1 1
75 #
76 # Contact tensile Layer 1
77 #       group          elty    flexcrossname   no    n1       n2      n3
      n4
78 Elcon   tenscontact1 hcont453 contmat1 50001    10001    10002   30001
      30002
79 #       n    elinc   nodinc
80 Repeat 200    1         1
81 # Contact tensile Layer 1-Layer2
82 #       group          elty    flexcrossname   no    n1       n2      n3
      n4
83 Elcon   tenscontact4 hcont453 contmat4 70001    30001    30002   40001
      40002
84 #       n    elinc   nodinc
85 Repeat 200    1         1
86 # Contact tensile Layer 2-outwards
87 #       group          elty    flexcrossname      no    n1     n2      n3
          n4
88 Elcon   tenscontact2 spring137     contmat2     60002    20002     40002
89 #       n    elinc   nodinc
90 Repeat 199    1         1
91 #
92 # Contact tensile Layer 2-outwards, ends
93 #       group          elty    flexcrossname      no    n1     n2      n3
          n4
94 Elcon   tenscontact3 spring137     contmat3     60001    20001    40001
95 #       n    elinc   nodinc
96 Repeat 2      200      200
97 #
98 # Contact tensile Layer 2-LOADS
```

```
#       group          elty    flexcrossname      no    n1     n2      n3
         n4
Elcon   tenscontact5 spring137     contmat5     80002    40002     80002
#        n    elinc   nodinc
Repeat 199    1         1
#
# Contact tensile Layer 2-LOADS, ends
#       group          elty    flexcrossname      no    n1     n2      n3
         n4
Elcon   tenscontact6 spring137     contmat6     80001    40001    80001
#        n    elinc   nodinc
Repeat 2      200      200
#-------------------------------------------------
# Orient input
#
# The core
#                          no      x  y     z
Elorient Coordinates      1       0  1e3     0
                          200     0  1e3     0
Elorient Coordinates      501     0  1e3     0
                          700     0  1e3     0
#
#                          no      x  y     z
# Tensile Layers
#                          no      x  y     z
Elorient Coordinates    30001      0  1e3     0
                        30200      0  1e3     0
Elorient Coordinates    40001      0  1e3     0
                        40200      0  1e3     0
# contact
elorient eulerangle 50001 0.0 0.0 0.0
                    50200 0.0 0.0 0.0
elorient eulerangle 70001 0.0 0.0 0.0
                    70200 0.0 0.0 0.0
elorient eulerangle 60001 0.0 0.0 0.0
                    60201 0.0 0.0 0.0

elorient eulerangle 80001 0.0 0.0 0.0
                    80201 0.0 0.0 0.0
#
#
#         groupn         mname        sname     is1 isn istx   isty istz
     gt1 gt2
#1 means that fric is independent(tape between layers) else (isotropic
     model)
CONTINT tenscontact1   core         tenslayer1 1    3   10.1   10.1   0    60
        2
CONTINT tenscontact4   tenslayer1   tenslayer2 1    3   10.1   10.1   0    60
        2
#-------------------------------------------------
# Element property input
#
#       name   type     rad   th   CDr   Cdt CMr CMt wd      ws      ODp     ODw
        rks
ELPROP core   pipe 0.1481 0.001 1.0 0.1 2.0 0.2 500.00 0.00   0.197
     0.197 0.5
ELPROP coreh pipe 0.0100 0.001 1.0 0.1 2.0 0.2 500.00 0.00   0.197
```

```
    0.197 0.5
148 #                                        b     t     md  ms scale thims
    thimd iop
149 #iop=1 turn off axisymm shear interaction=2 turn off bending shear
    interaction
150 ELPROP tenslayer1 shearhelix rectangle 0.010 0.003 0.2 0.0 74.0 200
    100    0
151 ELPROP tenslayer2 shearhelix rectangle 0.010 0.003 0.2 0.0 74.0 200
    100    0
152 #                                  gap0 tunetime AUTOMNPC autosearch
153 ELPROP tenscontact1  layercontact D D  D 0
154 ELPROP tenscontact4  layercontact D D  D 1
155 #                                  turnofftransformation   isotropic
    hardening
156 # isotropic hardening requires coulomb in material card
157 ELPROP tenscontact2  genspring  10.1   10.1   0   0   0   0 1       1
158 ELPROP tenscontact3  genspring  10.1   10.1   0   0   0   0 1       1
159 ELPROP tenscontact5  genspring  10.1   10.1   0   0   0   0 1       1
160 ELPROP tenscontact6  genspring  10.1   10.1   0   0   0   0 1       1
161 #          name   type        shearm
162 # Boundary condition data
163 #       Loc     node  dir
164 BONCON GLOBAL 101     1
165 BONCON GLOBAL 1       2 repeat 201 1
166 BONCON GLOBAL 1       3 repeat 201 1
167 BONCON GLOBAL 101     4
168 BONCON GLOBAL 1       5 repeat 201 1
169 BONCON GLOBAL 1       6 repeat 201 1
170 #
171 #
172 # fix the relative disp at ends
173 BONCON gLObAL 30001       1
174 BONCON gLObAL 30001       2
175 BONCON gLObAL 30001       4 repeat 201 1
176 # repeat 1616 1
177 BONCON gLObAL 30201       1
178 BONCON gLObAL 30201       2
179 #
180 BONCON gLObAL 40001       1
181 BONCON gLObAL 40001       2
182 BONCON gLObAL 40001       4 repeat 201 1
183 #repeat 1616 1
184 BONCON gLObAL 40201       1
185 BONCON gLObAL 40201       2
186 #
187 BONCON gLObAL 10001       1 repeat 201 1
188 BONCON gLObAL 10001       2 repeat 201 1
189 BONCON gLObAL 10001       3 repeat 201 1
190 BONCON gLObAL 10001       4 repeat 201 1
191 BONCON gLObAL 10001       5 repeat 201 1
192 BONCON gLObAL 10001       6 repeat 201 1
193 #
194 BONCON gLObAL 20001       1 repeat 201 1
195 BONCON gLObAL 20001       2 repeat 201 1
196 BONCON gLObAL 20001       3 repeat 201 1
197 BONCON gLObAL 20001       4 repeat 201 1
198 BONCON gLObAL 20001       5 repeat 201 1
```

```
199 BONCON gLObAL 20001       6 repeat 201 1
200 #
201 BONCON gLObAL 80001       1 repeat 201 1
202 BONCON gLObAL 80001       2 repeat 201 1
203 #BONCON gLObAL 80001       3 repeat 101 1
204 BONCON gLObAL 80001       4 repeat 201 1
205 BONCON gLObAL 80001       5 repeat 201 1
206 BONCON gLObAL 80001       6 repeat 201 1
207 #-------------------------------------------------
208 #
209 # Constraint input
210 CONSTR CONEQ GLOBAL   30002 3 0.0 30001 3 1.0 repeat 200 1 0
211 CONSTR CONEQ GLOBAL   40002 3 0.0 40001 3 1.0 repeat 200 1 0
212 #
213 #
214 #-------------------------------------------------
215 #  Material data
216 #         name      type   poiss talfa   tecond heatc beta    ea       eiy
          eiz
217 MATERIAL plastic   linear   0.0 11.7e-6   50    800    0   3.02e5   3.210e4
     3.210e4
218 #                              git       em      gm      den
219                             4.210e4    2.1e11  8e10     1000      2.1e11
220 #         name      type   poiss talfa   tecond heatc beta      ea      eiy
       eiz
221 MATERIAL plastich linear   0.0 11.7e-6    50      800    0     1000.0   0.0
       0.0
222 #                              git       em      gm      den
223                                0.0     2.1e11  8e10     0         2.1e11
224 #         name     type     poiss rho   talfa   tecond   heatc   eps sigma
225 MATERIAL tendon    elastic 0.3 7850 11.7e-6   50 800    2.1e11 8.076e10
     2.1e11
226 #         name         type         alfa    eps     sigma
227 MATERIAL shearmat   epcurve           1    0.0      0.00
228                                           0.2      0.9
229                                           1.0      1.0
230                                        1000.0      2.0
231 #-------------------------------------------------
232 #        Contact coil-swift:
233 #         name           type      rmyx   rmyz   xmat     ymat      zmat
234 MATERIAL contmat1 isocontact   #fric    bellx    bellz
235 MATERIAL contmat4 isocontact   #fric    bellx    bellz4
236 MATERIAL contmat2 genspring    bellx1   bellx1   bellz2   zero   zero   zero
       coulomb
237 MATERIAL contmat3 genspring    bellx1   bellx1   bellz3   zero   zero   zero
       coulomb
238 MATERIAL contmat5 genspring    bellx1   bellx1   bellz5   zero   zero   zero
       coulomb
239 MATERIAL contmat6 genspring    bellx1   bellx1   bellz6   zero   zero   zero
       coulomb
240 #         name       type      alfa    eps      sig
241 MATERIAL bellx      epcurve   1       0        0
242                                       0.0001     1.0
243                                       1000       2.5
244 #         name       type      alfa    eps      sig
245 MATERIAL bellx1      epcurve   1        0        0
246                                       0.0001     1.0*#fric
```

```
247                                          1000       3.0*#fric
248 #
249 MATERIAL belly      epcurve  1          0          0
250                                          1          1
251                                          1000       900
252 #
253 MATERIAL bellz      hycurve           -1000     -1.4e12
254                                          1000       1.4e12
255 MATERIAL bellz4      hycurve           -1000     -1.4e14
256                                          1000       1.4e14
257 #
258 MATERIAL bellz2     hycurve           -1000     0
259                                            0          0
260                                          0.001      1.72e5*#stiffred
261                                          1000       1.72e11*#stiffred
262 #
263 MATERIAL bellz3     hycurve           -1000     0
264                                            0          0
265                                          0.001      1.72e5*0.5*#stiffred
266                                          1000       1.72e11*0.5*#stiffred
267 #
268 MATERIAL bellz5     hycurve           -1000     -1E6
269                                            0          0
270                                          1000       0
271 #
272 MATERIAL bellz6     hycurve           -1000     -1E6/2
273                                            0          0
274                                          1000       0
275 #
276 MATERIAL zero     hycurve           -1000     0
277                                          1000     0
278 #
279
280 #          name           type      rmyx  rmyz  xmat     ymat      zmat
281 #MATERIAL contmat   contact   0.30   0.60   bellx    belly     bellz
282 #
283 TIMECO     1.0   0.1   1.0   101.0   dynamic   auto   none    disp   15   5    1e
        -5
284 TIMECO    101.0   0.1   1.0   101.0   dynamic   auto   go-on   disp   15   5    1
        e-5
285 #-------------------------------------------------
286 # Load input
287 CONSTR pdisp global    201 1 #pdispfac 300
288 CONSTR pdisp global      1   1 -#pdispfac 300
289 #-------------------------------------------------
290 # Cload input
291 #
292 #      hist   dir   no1 r1   no2 r2          n m
293 #
294 CLOAD   400     3     80001   -4.772e4/4
295 CLOAD   400     3     80201   -4.772e4/4
296 CLOAD   400     3     80002   -4.772e4/2 80200 -4.772e4/2
297 #-------------------------------------------------
298 PELOAD 200 100
299 #-------------------------------------------------
300 # drymass
301  THIST_R 100   0.0           10.0 rampcos 1.0
```

```
# buoyancy
 THIST 200   0            0.0
               1            0.00
              10            0.00
              20            0.00
             100            0.00
# inistr x-dir
 THIST 300   0           0.0
              20           0.0
              101          -0.025
# external pressure
 THIST_R 400    0             10.0 rampcos 0.0
              10.0           20.0 rampcos #pext
```

D Matrixplot inputfile: mplot_oc.2bpi

To generate plots the program BFLEX2010Post has been used. The input file for this program looks like this:

```
1  NOPLOT "input" "mplot_oc-nodispx" "Time" TIME "Strain (-)"
       nodisp-x 201 201 1 200/4.9837
2  GLPLOT "input" "mplot_oc-axfor-core" "X-COORD(m)" E-COR "
     Force" elforce-x 1 200 1 1e-3 1
3  GLPLOT "input" "mplot_oc-condisy-c1" "X-COORD(m)" E-COR "Y-
     COORD(m)" condis-Y 50001 50200 1 1 1
4  GLPLOT "input" "mplot_oc-condisy-12" "X-COORD(m)" E-COR "
     Y-COORD(m)" condis-Y 70001 70200 1 1 1
5  GLPLOT "input" "mplot_oc-confory-c1" "X-COORD(m)" E-COR "
     Y-COORD(m)" confor-Y 50001 50200 1 1 1
6  GLPLOT "input" "mplot_oc-confory-12" "X-COORD(m)" E-COR "
     Y-COORD(m)" confor-Y 70001 70200 1 1 1
7  ELPLOT "input" "mplot_oc-epsxx" "Time (s)" TIME "eps-xx-core (-)
     " ELFORCE-X 100 100 1 3.3e-6*100 1
8  ELPLOT "input" "mplot_oc-forcx-core" "Time (s)" TIME "Force-x
     -core (MN)" ELFORCE-X 100 100 1 1e-6 1
9  ELPLOT "input" "mplot_oc-forcx-lay1" "Time (s)" TIME "
     Force-x-layer1 (MN)" ELFORCE-X 30100 30100 1 1e-6 1
10 ELPLOT "input" "mplot_oc-forcx-lay2" "Time (s)" TIME "
     Force-x-layer2 (MN)" ELFORCE-X 40100 40100 1 1e-6 1
11 ELPLOT "input" "mplot_oc-forcy-lay1" "Time (s)" TIME "
     Force-y-layer1 (MN)" ELFORCE-y 30100 30100 1 1e-6
       1
12 ELPLOT "input" "mplot_oc-forcy-lay2" "Time (s)" TIME "
     Force-y-layer2 (MN)" ELFORCE-y 40100 40100 1 1e-6
     1
13 GLPLOT "input" "mplot_oc-mz-lay1" "X-COR (m)" E-COR
       "M-z-layer1 (-)" ELMOM-Z 30001 30200 1 1e-3
         1
14 GLPLOT "input" "mplot_oc-mz-lay2" "X-COR (m)" E-COR
       "M-z-layer2 (-)" ELMOM-Z 40001 40200 1 1e-3
         1
15 GNPLOT "input" "mplot_oc-norotz-inner" "Number of pitches" X
     -COR "Theta_z [rad]" NOROT-Z 30001 30200 0.602 1
16 GNPLOT "input" "mplot_oc-norotz-outer" "Number of pitches" X
     -COR "Theta_z [rad]" NOROT-Z 40001 40200 0.602 1
17 GLPLOT "input" "mplot_oc_cz_spring" "X coordinate" E-
     COR "Cont z" CONFOR-Z 60002 60200 1.0 1.0
18 ELPLOT "input" "mplot_oc-epsxx-lay1" "Time (s)" TIME
       "eps-xx-layer1 (-)" ELFORCE-X 30100 30100 1
       2.59e-9 1
```

E Modifications of the BFLEX2010 input file

When applying the external pressure in different ways the input file for BFLEX2010 must be modified. Using the file specified in Appendix C as a basis the following changes must be made for the different cases:

Case 2

The following lines has to be removed:

```
100 Elcon   tenscontact5  spring137     contmat5     80002    40002     80002

106 Elcon   tenscontact6  spring137     contmat6     80001    40001     80001

270                                       1000         0

274                                       1000         0

294 CLOAD   400      3     80001    -4.772e4/4
295 CLOAD   400      3     80201    -4.772e4/4
296 CLOAD   400      3     80002    -4.772e4/2  80200  -4.772e4/2
```

The following lines must be added:

```
100 Elcon   tenscontact3  spring137     contmat3     60001    20001     40001

106 Elcon   tenscontact5  spring137     contmat5     80002    30002     80002

270                                       1000         1E6

274                                       1000         1E6/2

294 CLOAD   400      3     80001    4.772e4/4
295 CLOAD   400      3     80201    4.772e4/4
296 CLOAD   400      3     80002    4.772e4/2  80200  4.772e4/2
```

Case 3

The following lines has to be removed:

```
31 Nocoor Polar
32 #    x0     y0    z0    b1    b2    b3    R
33      0.0    0.0   0.0   0.0   0.0   0.0   0.2993/2
34 #    node     xcor      theta
35      30001  0.00     3.1416
36      30201  4.9837   -16.0984
```

```
100 Elcon   tenscontact5  spring137     contmat5     80002    40002     80002
101 #         n    elinc   nodinc
102 Repeat 199    1          1
103 #
104 # Contact tensile Layer 2-LOADS, ends
105 #       group           elty    flexcrossname      no    n1     n2      n3
          n4
106 Elcon   tenscontact6  spring137     contmat6     80001    40001    80001
107 #         n    elinc   nodinc
108 Repeat 2      200       200
```

```
134 elorient eulerangle 80001 0.0 0.0 0.0
135                     80201 0.0 0.0 0.0
```

```
159 ELPROP tenscontact5   genspring   10.1    10.1    0    0    0    0 1        1
160 ELPROP tenscontact6   genspring   10.1    10.1    0    0    0    0 1        1
```

```
201 BONCON gLObAL 80001       1 repeat 201 1
202 BONCON gLObAL 80001       2 repeat 201 1
203 #BONCON gLObAL 80001       3 repeat 101 1
204 BONCON gLObAL 80001       4 repeat 201 1
205 BONCON gLObAL 80001       5 repeat 201 1
206 BONCON gLObAL 80001       6 repeat 201 1
```

```
238 MATERIAL contmat5 genspring    bellx1   bellx1   bellz5   zero   zero   zero
      coulomb
239 MATERIAL contmat6 genspring    bellx1   bellx1   bellz6   zero   zero   zero
      coulomb
```

```
268 MATERIAL bellz5     hycurve        -1000    -1E6
269                                      0        0
270                                   1000        0
271 #
272 MATERIAL bellz6     hycurve        -1000    -1E6/2
273                                      0        0
274                                   1000        0
```

```
294 CLOAD   400     3     80001   -4.772e4/4
295 CLOAD   400     3     80201   -4.772e4/4
296 CLOAD   400     3     80002   -4.772e4/2 80200 -4.772e4/2
```

The following has to be added

```
294 #                    noideid      dof      dispval      histno
295 CONSTR pdisp global    20001        3        -4.9064e-04          400
296 repeat 201 1
```

Case 4

The following line must be removed:

```
167 BONCON GLOBAL 101      4
```

The following line must be added:

```
167 BONCON GLOBAL 1        4 repeat 201 1
```

Case 5

Remove and add lines as mentioned in Appendix E Case 2 and Appendix E Case 4.

Case 6

Remove and add lines as mentioned in Appendix E Case 3 and Appendix E Case 4.

F Matlabscript : amultiscan.m

Matlabscript used to read the result files from BFLEX2010Post and generate of multiple analyses in the same chart.

```
1
2  nant = 20;
3  pext1 = 2;
4  pext2 = 4;
5
6  y = []; y1 = []; y2 = []; ysum = []; x = []; x1 = []; x2 = []; l = [];
7  plength = []; plength1 = []; plength2 = [];
8  deltaeps = []; endshort = []; kforcefac = zeros(nant,1);
9
10 nyvaz32 = 'Multi_Adjusted_Endshort_vs_Force_';
11 analysenavn = 'analyse';
12 mpf = '.mpf'; jpg = '.jpeg'; png = '.png'; mpa = 'MPa'; nr = '_nr';
13 pres1 = num2str(pext1); pres2 = num2str(pext2);
14
15 for j = 1:nant
16
17 fid = 0; fad = 0; fud = 0; fed = 0; fod = 0;
18 tall = j; mappenr = num2str(j);
19 mappenavn = [analysenavn mappenr];
20
21 grafnavn1 = [mappenavn '/matrixplots_original/mplot_oc-forcx-core.mpf'
       ];
22 grafnavn2 = [mappenavn '/matrixplots_original/mplot_oc-forcx-lay1.mpf'
       ];
23 grafnavn3 = [mappenavn '/matrixplots_original/mplot_oc-forcx-lay2.mpf'
       ];
24 grafnavn4 = [mappenavn '/matrixplots_original/mplot_oc-nodispx.mpf'];
25 grafnavn6 = [mappenavn '/matrixplots_original/mplot_oc-epsxx.mpf'];
26
27 fid = fopen(grafnavn1,'rt');  fad = fopen(grafnavn2,'rt');
28 fud = fopen(grafnavn3,'rt');  fed = fopen(grafnavn4,'rt');
29 fod = fopen(grafnavn6,'rt');
30
31 nLines = 0;
32 while (fgets(fid) ~= -1),
33   nLines = nLines+1;
34 end
35 plength(j) = nLines-9;
36 nLines1 = 0;
37 while (fgets(fad) ~= -1),
38   nLines1 = nLines1+1;
39 end
40 plength1(j) = nLines1-9;
41 nLines2 = 0;
42 while (fgets(fud) ~= -1),
43   nLines2 = nLines2+1;
44 end
45 plength2(j) = nLines2-9;
46
47 fseek(fid,0,-1); fseek(fid,8,'cof'); fseek(fad,0,-1); fseek(fad,8,'cof
       ');
48 fseek(fud,0,-1); fseek(fud,8,'cof'); fseek(fed,0,-1); fseek(fed,8,'cof
```

```
    ');
fseek(fod,8,'cof'); teller = 0;

for i = 1:nLines

    if i < 9
        tstring = fgets(fid); tstring1 = fgets(fad);
        tstring2 = fgets(fud); dxstring = fgets(fed);
        cxstring = fgets(fod);
    else
        teller = teller + 1; nstring = fgets(fid);
        nstring1 = fgets(fad); nstring2 = fgets(fud);
        if teller == 1
            x(j,teller) = 0.1; x1(j,teller) = 0.1;
            x2(j,teller) = 0.1;
        else
            x(j,teller) = teller-1; x1(j,teller) = teller-1;
            x2(j,teller) = teller-1;
        end
        yc = nstring(27:38); yc1 = nstring1(27:38);
        yc2 = nstring2(27:38);

        y(j,teller) = str2num(yc); y1(j,teller) = str2num(yc1);
        y2(j,teller) = str2num(yc2);

        dstring = fgets(fed); lc = dstring(27:38);
        l(j,teller) = str2num(lc);

        cstring = fgets(fod); cc = cstring(27:38);
        ce(j,teller) = str2num(cc);

        sign = nstring(26); sign1 = nstring1(26);
        sign2 = nstring2(26); sign3 = dstring(26);
        sign5 = cstring(26);

        if sign == '-'
            y(j,teller) = y(j,teller) * -1;
        end
        if sign1 == '-'
            y1(j,teller) = y1(j,teller) * -1;
        end
        if sign2 == '-'
            y2(j,teller) = y2(j,teller) * -1;
        end
        if sign3 == '-'
            l(j,teller) = l(j,teller) * -1;
        end
        if sign5 == '-'
            ce(j,teller) = ce(j,teller) * -1;
        end
        ysum(j,teller) = y(j,teller)+y1(j,teller)+y2(j,teller);
    end

end
end

l = abs(l); ce = abs(ce);
```

```
105 maxvalue = zeros(nant,1); maxcoord = zeros(nant,1);
106
107 for j = 1:nant
108
109     [m,n] = size(ysum);
110
111     maxcoord(j,1) = 1; maxvalue(j,1) = ysum(j,1);
112     maxdispcord(j,1) = 1; maxdisp(j,1) = ce(j,1);
113     buckle = 0;
114     for i = 2:n
115     if ysum(j,i) >= maxvalue(j,1) && buckle == 0
116         maxcoord(j,1) = i;
117         maxvalue(j,1) = ysum(j,i);
118         if i < 102
119         if ysum(j,i+1) < ysum(j,i)
120             buckle = 1;
121         end
122         end
123     end
124     if ce(j,i) >= maxdisp(j,1) && i <= maxcoord(j,1)
125         maxdisp(j,1) = ce(j,i);
126         maxdispcord(j,1) = i;
127     end
128     end
129     if maxvalue(j,1) < 0.5
130     evalue(j,:) = [ce(j,maxcoord(j,1)) ce(j,maxcoord(j,1)) ce(j,
        maxcoord(j,1)) ce(j,maxcoord(j,1)) ce(j,maxcoord(j,1))];
131     else
132     evalue(j,:) = [ce(j,maxcoord(j,1)) ce(j,maxcoord(j,1)) ce(j,
        maxcoord(j,1)) ce(j,maxcoord(j,1)) ce(j,maxcoord(j,1))];
133     end
134 end
135
136 for j = 1:nant
137         deltaepsilon = ce(10,22);
138         kforcefac = y1(10,21)/(y1(10,31)-y1(10,21));
139         deltaeps = deltaepsilon*kforcefac;
140         for i = 1:10
141             endshort(j,i+11) = ce(j,i+11) + 0.1*i*deltaeps(1,1);
142         end
143         for i = 22:plength(j)
144             endshort(j,i) = ce(j,i) + deltaeps(1,1);
145         end
146
147     for i = 1:5
148     modevalue(j,i) = evalue(j,i) + deltaeps(1,1);
149     end
150 end
151
152 set(0,'DefaultAxesColorOrder',[0 0 0;1 0.5 0;0 0 1;56/255 176/255
    222/255; 255/255 20/255 147/255; 1 1 0; 160/255 32/255 240/255;
    139/255 69/255 19/255; 1 0 0; 0 1 0],...
153       'DefaultAxesLineStyleOrder',{'-','--'})
154
155 maxdispcord = maxdispcord-1;
156
157 for j = 1:nant
```

```
158     vline = endshort(j,maxdispcord(j,1));
159     vlinevalue = ysum(j,maxdispcord(j,1));
160     vlinex(j,:) = [vline vline vline vline vline];
161     vliney(j,:) = [vlinevalue vlinevalue-0.05 vlinevalue-0.1
            vlinevalue-0.15 vlinevalue-0.2];
162 end
163
164     plot(vlinex(1,:),vliney(1,:),'s-',vlinex(2,:),vliney(2,:),'o-',
            vlinex(3,:),vliney(3,:),'^-',vlinex(4,:),vliney(4,:),'v-',
            vlinex(5,:),vliney(5,:),'<-',vlinex(6,:),vliney(6,:),'>-',
            vlinex(7,:),vliney(7,:),'d-',vlinex(8,:),vliney(8,:),'p-',
            vlinex(9,:),vliney(9,:),'h-',vlinex(10,:),vliney(10,:),'*-')
165     hold on
166     plot(endshort(1,1:maxdispcord(1)),ysum(1,1:maxdispcord(1)),
            endshort(2,1:maxdispcord(2)),ysum(2,1:maxdispcord(2)),endshort
            (3,1:maxdispcord(3)),ysum(3,1:maxdispcord(3)),endshort(4,1:
            maxdispcord(4)),ysum(4,1:maxdispcord(4)),endshort(5,1:
            maxdispcord(5)),ysum(5,1:maxdispcord(5)),endshort(6,1:
            maxdispcord(6)),ysum(6,1:maxdispcord(6)),endshort(7,1:
            maxdispcord(7)),ysum(7,1:maxdispcord(7)),endshort(8,1:
            maxdispcord(8)),ysum(8,1:maxdispcord(8)),endshort(9,1:
            maxdispcord(9)),ysum(9,1:maxdispcord(9)), endshort(10,1:
            maxdispcord(10)),ysum(10,1:maxdispcord(10)))
167     axis('tight');
168     ttekst1 = 'BFLEX 2010 - End shortening versus axial force all
            layers - External pressure ';
169     trykk1 = num2str(pext1);
170     ttekst2 = ' MPa';
171     title([ttekst1 trykk1 ttekst2],'FontSize',12)
172     legend('0.00','0.01','0.02','0.04','0.06','0.08','0.10','0.15','
            0.20','0.40','Location', 'NorthWest');
173     xlabel('End shortening (%\DeltaL/L)','FontSize',12)
174     ylabel('Force [MN]','FontSize',12)
175     multiname3 = [nyvaz32 trykk1 ttekst2 png];
176     print(gcf,'-dpng',[multiname3],'-r600')
177
178     if nant > 10
179     plot(vlinex(11,:),vliney(11,:),'s-',vlinex(12,:),vliney(12,:),'o-'
            ,vlinex(13,:),vliney(13,:),'^-',vlinex(14,:),vliney(14,:),'v-'
            ,vlinex(15,:),vliney(15,:),'<-',vlinex(16,:),vliney(16,:),'>-'
            ,vlinex(17,:),vliney(17,:),'d-',vlinex(18,:),vliney(18,:),'p-'
            ,vlinex(19,:),vliney(19,:),'h-',vlinex(20,:),vliney(20,:),'*-'
            )
180     hold on
181     plot(endshort(11,1:maxdispcord(11)),ysum(11,1:maxdispcord(11)),
            endshort(12,1:maxdispcord(12)),ysum(12,1:maxdispcord(12)),
            endshort(13,1:maxdispcord(13)),ysum(13,1:maxdispcord(13)),
            endshort(14,1:maxdispcord(14)),ysum(14,1:maxdispcord(14)),
            endshort(15,1:maxdispcord(15)),ysum(15,1:maxdispcord(15)),
            endshort(16,1:maxdispcord(16)),ysum(16,1:maxdispcord(16)),
            endshort(17,1:maxdispcord(17)),ysum(17,1:maxdispcord(17)),
            endshort(18,1:maxdispcord(18)),ysum(18,1:maxdispcord(18)),
            endshort(19,1:maxdispcord(19)),ysum(19,1:maxdispcord(19)),
            endshort(20,1:maxdispcord(20)),ysum(20,1:maxdispcord(20)))
182     axis('tight');
183     ttekst1 = 'End shortening versus axial force all layers - External
             pressure ';
```

```
184     trykk2 = num2str(pext2);
185     ttekst2 = ' MPa';
186     moretext = ' and ';
187     title([ttekst1 trykk1 moretext trykk2 ttekst2],'FontSize',12)
188     legend('0.00','0.01','0.02','0.04','0.06','0.08','0.10','0.15','
            0.20','0.40','Location', 'NorthWest');
189     xlabel('End shortening (%\DeltaL/L)','FontSize',12)
190     ylabel('Force [MN]','FontSize',12)
191     multiname3 = [nyvaz32 trykk2 ttekst2 png];
192     print(gcf,'-dpng',[multiname3],'-r600')
193     hold off
194     end
```